

RESEARCH ARTICLE

WFDC3 identified as a prognostic and immune biomarker in pancreatic cancer

Bohan Liu ¹, Xuqing Shi ¹, Tianqi Liu ^{2*}, Huanwen Wu ^{2*}, and Zhiyong Liang ^{2*}

The whey acidic protein four-disulfide core (WFDC) family comprises key modulators of tumor initiation and progression, offering significant potential for diagnostic, prognostic, and therapeutic applications. However, the specific role of WFDCs in the oncogenesis of pancreatic cancer (pancreatic adenocarcinoma [PAAD]) remains incompletely understood. To address this, we conducted an initial investigation using comprehensive bioinformatic analyses to evaluate *WFDCs* expression patterns across multiple tumor types, with a focus on PAAD. Bulk and single-cell RNA sequencing datasets from the TCGA and GEO repositories were analyzed to assess *WFDC3* expression in PAAD tissues. Kaplan–Meier survival analysis was employed to determine the prognostic significance of *WFDC3*. To explore its biological functions and underlying mechanisms, we performed functional enrichment analyses in combination with immune infiltration assessments. Experimental validation included CCK-8 and EdU proliferation assays, transwell migration and invasion tests, immunofluorescence staining, flow cytometry, LDH release assays, Western blotting, and quantitative reverse transcription PCR. A LASSO regression model was also developed to predict PAAD outcomes. Our findings reveal that WFDCs exhibit context-dependent roles in tumor progression. Specifically, *WFDC3* expression was significantly elevated in PAAD and associated with poorer patient prognosis. Functionally, *WFDC3* promoted PAAD cell metastasis by inducing epithelial–mesenchymal transition and contributed to immune evasion by suppressing T cell cytotoxicity. In conclusion, our study identifies *WFDC3* as a pro-oncogenic factor in PAAD progression, highlighting its potential as both a prognostic biomarker and a therapeutic target for regulating metastasis and immune responses in this malignancy.

Keywords: Pancreatic cancer, whey acidic protein four-disulfide core, *WFDC3*, bioinformatics, metastasis, immunotherapy, prognosis.

Introduction

Pancreatic cancer (pancreatic adenocarcinoma [PAAD]) is an aggressive malignancy that presents significant challenges in both diagnosis and treatment, primarily due to its insidious onset, high metastatic potential, and the limited efficacy of current therapeutic strategies [1]. Epidemiological data show that PAAD has nearly identical incidence and mortality rates, with a dismal five-year survival rate of approximately 10% [2, 3]. This clinical reality underscores the urgent need for novel biomarkers capable of predicting outcomes, monitoring recurrence, and identifying therapeutic targets. Although recent advances in immunotherapy have shown promising efficacy in various cancer types, their clinical benefit for PAAD patients remains substantially limited [4]. Evidence suggests that the pancreatic tumor microenvironment is enriched with immunosuppressive cells and factors that collectively impair effective immune responses [5]. Therefore, characterizing this immunosuppressive microenvironment is crucial for identifying new immunotherapeutic targets in PAAD. The whey acidic

protein four-disulfide core (WFDC) family comprises 18 distinct genes, 14 of which are located on human chromosome 20. Most members encode secretory proteins of relatively small molecular weight [6]. These proteins are defined by the presence of one or more WFDC domains, featuring conserved structural motifs of 40–50 amino acids, within which eight cysteine residues form four disulfide bridges through specific bonding patterns [7, 8]. WFDC proteins are broadly expressed across human tissues—particularly in the reproductive and respiratory systems—where they participate in diverse biological processes, including protease inhibition, antimicrobial activity, and immune modulation [9]. Dysregulated WFDC expression has been significantly associated with various pathological conditions, especially in the development and metastatic progression of several malignancies [10–12], highlighting the need for systematic, multi-omics studies of WFDCs in pan-cancer contexts. WFDCs exhibit cancer type-dependent functional diversity, reflecting their heterogeneous biological roles in malignant conditions. Elevated serum levels of

¹Molecular Pathology Research Center, Department of Pathology, Peking Union Medical College Hospital, Chinese Academy of Medical Sciences and Peking Union Medical College, Beijing, China; ²Department of Pathology, State Key Laboratory of Complex Severe and Rare Disease, Molecular Pathology Research Center, Peking Union Medical College Hospital, Chinese Academy of Medical Sciences and Peking Union Medical College, Beijing, China.

*Correspondence to Zhiyong Liang: liangzy@pumch.cn; Huanwen Wu: wuhuanwen10700@pumch.cn and Tianqi Liu: liutianqi49@pumch.cn

DOI: 10.17305/bb.2025.12444

© 2025 Liu et al. This article is available under a Creative Commons License (Attribution 4.0 International, as described at <https://creativecommons.org/licenses/by/4.0/>).

WFDC2 have been validated as clinically relevant biomarkers for diagnostic evaluation and prognostic stratification in lung cancer [13]. In ovarian carcinoma, WFDC2 has emerged as a biomarker with high diagnostic accuracy across multiple clinical studies [14]. Conversely, prostate cancer specimens often show significant downregulation of WFDC2, correlating inversely with Gleason grade parameters [15]. Previous research from our group identified a tumor-suppressive role of WFDC3 in inhibiting estrogen-dependent metastasis via activation of the ER β /TGFBR1 pathway [16]. Additionally, we found that WFDC3 serves as a predictive marker for enhanced chemotherapeutic response in colorectal cancer (CRC), through modulation of the ATM/ATR kinase signaling pathways [17]. Nevertheless, the pathophysiological relevance of WFDC3 in other malignancies—particularly PAAD—remains insufficiently explored and warrants further mechanistic investigation.

In this study, we conducted a comprehensive pan-cancer analysis to evaluate the expression patterns of WFDCs and their correlations with the immune microenvironment across 33 malignancies, using bulk RNA-seq datasets from the TCGA and GTEx repositories. We then focused specifically on WFDC3 expression in PAAD, utilizing both bulk transcriptomic and single-cell RNA sequencing (scRNA-seq) data to elucidate associated molecular pathways. Through a combination of computational analyses and experimental validation, we found that WFDC3 expression was significantly elevated in PAAD specimens and that higher expression levels were strongly associated with poor clinical outcomes. Notably, our study is the first to demonstrate that WFDC3 knockdown markedly suppresses tumor cell invasion and migration while enhancing susceptibility to immune-mediated cytotoxicity. Finally, we developed a WFDCs-based prognostic signature to stratify survival outcomes in PAAD patients. Together, these findings highlight the dual role of WFDCs as both prognostic biomarkers and promising therapeutic targets in PAAD management.

Materials and methods

Genomic data and clinical information

Transcriptomic profiles, clinicopathological parameters, and somatic mutation datasets for 33 solid tumors were obtained from the TCGA database (<https://portal.gdc.cancer.gov/>) and the UCSC Xena platform (<https://xena.ucsc.edu/>). Corresponding normal tissue transcriptomic data were sourced from the GTEx project (<https://commonfund.nih.gov/GTEx>) for comparative analysis. FPKM values were normalized to TPM to enable unbiased comparisons. To correct for potential batch effects arising from the integration of TCGA and GTEx datasets, we applied the ComBat_seq function from the “sva” R package, which adjusts for known batch variables in RNA-seq count data while preserving biological signals. Data preprocessing included the exclusion of non-compliant records with missing entries or duplicates, followed by data visualization using the “ggplot2” package (v3.4.4) in the R programming environment.

Expression and prognostic analysis

The TIMER platform (<https://cistrome.shinyapps.io/timer/>) and the GEPIA database (<http://gepia.cancer-pku.cn/>) were utilized as primary analytical tools to investigate WFDCs expression patterns across various cancer types. Prognostic evaluation of WFDCs in pan-cancer contexts was conducted using the GSCA resource (<https://guolab.wchscu.cn/GSCA>). TCGA and GTEx datasets were subsequently used to validate the expression characteristics of WFDCs specifically in PAAD. The CRC immunotherapy cohort GSE53127 was obtained from the GEO database for further analysis. Kaplan–Meier survival curves were generated using the “survival” (v3.3.1) and “survminer” (v0.4.9) R packages to illustrate the associations of WFDCs with overall survival (OS), disease-specific survival (DSS), and progression-free interval (PFI) in PAAD. Additionally, the Kaplan–Meier method combined with univariate Cox regression analysis was applied to assess the prognostic significance of WFDC3 in relation to OS, DSS, and PFI across multiple cancer types.

scRNA-seq analysis

Initial investigation of WFDC3 expression patterns at single-cell resolution across diverse cell types in PAAD was conducted using the TISCH database (<http://tisch.comp-genomics.org/>). Transcriptomic data for WFDC3 mRNA levels were obtained from the GSE154778 dataset in the GEO repository (<https://www.ncbi.nlm.nih.gov/geo/>), and subsequently processed using Python 3.12.2 with Scanpy (v1.10.2) [18]. Dimensionality reduction was performed via principal component analysis, and batch effect correction was applied using the “scvi-tools” Python package (v1.2.0) [19, 20]. Cellular subpopulations were identified using the Leiden clustering algorithm on UMAP-transformed data, with cell type annotation based on known marker genes. Malignant cells were distinguished through chromosomal instability profiling using the “infercnvpy” Python package (v0.5.0) for single-cell CNV analysis. The spatial distribution and expression intensity of WFDC3 were visualized using UMAP projections and violin plots. Independent validation was conducted by re-analyzing the original scRNA-seq dataset with the Seurat analytical pipeline.

Clinicopathological and mutational analysis

Clinical and pathological features, along with somatic mutation profiles for 178 PAAD patients, were obtained from the TCGA-PAAD cohort. The associations between these features, genomic mutations, and WFDC3 expression were subsequently evaluated using the Mann–Whitney *U* test.

Identification of differentially expressed genes (DEGs) and functional enrichment analysis

To investigate biological processes and signaling pathways associated with WFDC3 expression, differential mRNA analysis was first conducted between WFDC3-low and WFDC3-high subgroups using TCGA-PAAD transcriptomic datasets via the “DESeq2” R package (v1.36.0). Significantly dysregulated genes were visualized using MA plots, applying predefined thresholds of adjusted *P* value (*p*_{adj}) < 0.05 and

absolute \log_2 fold change ($|\log_2FC| > 1$). Functional enrichment analyses were subsequently performed using the “ClusterProfiler” R package (v4.4.4) to identify enriched Gene Ontology (GO) terms and Kyoto Encyclopedia of Genes and Genomes (KEGG) pathways, with statistical significance set at $p_{adj} < 0.05$. To compare signaling pathway differences between *WFDC3* expression subgroups, Gene Set Enrichment Analysis (GSEA) was conducted using hallmark gene sets (h.all.v7.5.1.symbols.gmt) and immunologic signature collections (c7.all.v2022.1.Hs.symbols.gmt).

Tumor microenvironment and immune infiltration analysis

Immune infiltration scores for TCGA-PAAD cohort samples were calculated using the CIBERSORT computational method [21]. Comparative analysis revealed differences in immune cell composition between PAAD patients stratified by *WFDC3* expression levels, with results visualized using the “ggplot2” package. Stromal and immune cell proportions within the PAAD tumor microenvironment were estimated using the ESTIMATE algorithm to assess tumor purity [22]. To explore the relationship between *WFDC3* expression and T lymphocyte subpopulations, ssGSEA was performed using the “GSVA” R package (v1.46.0) [23, 24].

Development and validation of a prognostic model based on *WFDC3*s

A LASSO regression approach was implemented using the “glmnet” R package (v4.1.7) to evaluate 18 *WFDC* family members, with the optimal regularization parameter (λ) determined through cross-validation. Model construction utilized ten-fold cross-validation to ensure robustness and predictive generalizability. Four *WFDC* members (*WFDC3*, *WFIKKN1*, *SLPI*, *PI3*) showing significant associations with OS were incorporated into the prognostic signature. Risk stratification was based on the following formula: Risk Score = $(0.068 \times WFDC3) + (-0.5398 \times WFIKKN1) + (0.041 \times PI3) + (0.0738 \times SLPI)$, enabling classification of patients into low- and high-risk groups using the median risk score as a threshold. Model validation included Kaplan–Meier survival curves, ROC analysis, calibration plots, univariate forest plots, and prognostic nomogram construction to assess clinical predictive accuracy in PAAD. To explore immune landscape differences, Spearman’s rank correlation analysis was performed to compare immune cell infiltration patterns between risk groups. To strengthen the prognostic model’s credibility, external validation was conducted using two independent PAAD cohorts from the GEO database (GSE62452 and GSE78229). Expression levels of the four genes were normalized, and individual risk scores were calculated using the established formula. Patients were stratified into high- and low-risk groups based on the median score, and survival differences were assessed via Kaplan–Meier analysis.

Cell culture and cell transfection

The human pancreatic ductal epithelial cell line HPNE, the human T cell line Jurkat, and the human pancreatic cancer cell lines MIA PaCa-2, PANC-1, AsPC-1, and BxPC-3 were obtained from the American Type Culture Collection (ATCC). MIA PaCa-2 and PANC-1 cells were cultured in Dulbecco’s Modified Eagle’s

Medium (DMEM; Thermo Fisher Scientific, Waltham, MA, USA), while AsPC-1, BxPC-3, and Jurkat T cells were maintained in Roswell Park Memorial Institute Medium 1640 (RPMI-1640; Thermo Fisher Scientific, Waltham, MA, USA). All culture media were supplemented with 10% fetal bovine serum (FBS). HPNE cells were cultured in a customized medium consisting of 75% low-glucose DMEM and 25% Medium M3 Base (both from Thermo Fisher Scientific), supplemented with 5% FBS, 10 ng/mL human recombinant epidermal growth factor (EGF; PeproTech, NJ, USA), and 750 ng/mL puromycin. All cell lines were maintained at 37 °C in a humidified atmosphere containing 5% CO₂, with regular medium replacement and passaging according to standard protocols. For gain- and loss-of-function experiments, a *WFDC3* overexpression plasmid (GeneChem Co., Ltd., China) was transfected into PANC-1 cells using Lipofectamine 3000 reagent (Invitrogen, Catalog No. 3000155) at 80%–90% confluency. For gene knockdown, ON-TARGETplus SMARTpool *WFDC3* siRNA (Dharmacon, Catalog No. L-003402-00-0005, USA), a mixture of four siRNAs targeting *WFDC3*, was transfected into MIA PaCa-2 cells during the logarithmic growth phase using Lipofectamine RNAiMAX reagent (Invitrogen, Catalog No. 13778) at 70%–80% confluency, following the manufacturer’s protocol.

Enzyme-linked immunosorbent assay (ELISA)

WFDC3 protein levels in conditioned medium were quantified using a human-specific ELISA kit (Yuanju Biotechnology Co., Ltd., cat. YJ290758, Shanghai, China). Standard solutions, serum samples, and HRP-conjugated antigens were added to pre-coated assay plates according to the manufacturer’s instructions. After a 30-min incubation at 37 °C, residual liquid was discarded, and the plates were washed five times. Then, 50 μ L of TMB substrate was added and incubated in the dark at 37 °C for 10 min. The reaction was stopped by adding 50 μ L of stop buffer, and absorbance was measured immediately at 450 nm.

Cell viability and proliferation assay

Multiple experimental approaches were used to assess the proliferative capacity of PANC-1 cells following transfection with the *WFDC3* overexpression plasmid. Cell viability was measured at defined time points using the Cell Counting Kit-8 (Dojindo, Kumamoto, Japan). Colony formation was analyzed by fixing and staining cells with 0.5% crystal violet, followed by digital image capture. EdU incorporation assays were performed using the Cell-Light EdU Apollo643 *In Vitro* Kit (Ribobio, #C10310-2), according to the manufacturer’s protocol. Fluorescent signals were then acquired and quantified using High Content Analysis (HCA) instrumentation.

Transwell migration and invasion assay

Transwell chambers were employed for migration and invasion assays. For the invasion assay, the upper surfaces of the Transwell inserts were uniformly coated with extracellular Matrigel diluted 1:10. Differentially treated PAAD cells (5×10^4), suspended in 100 μ L of serum-free medium, were seeded into the coated upper chambers. The lower chambers of 24-well plates were filled with 500 μ L of complete medium containing 10%

FBS and incubated at 37 °C with 5% CO₂ for 24–48 h. Cells were fixed with 4% paraformaldehyde, and invasion was quantified using crystal violet staining. Membranes were imaged via bright-field microscopy, and cell counts were performed using ImageJ software.

Immunofluorescence (IF) staining

Cells were seeded onto glass coverslips and subjected to experimental treatments. After fixation, the slides were blocked with goat serum and incubated overnight at 4 °C with primary antibodies: E-cadherin (1:200, #14472S; CST, USA), N-cadherin (1:1000, #14215; CST, USA), and ZO-1 (1:200, #13663; CST, USA). Following washes, slides were incubated at room temperature for 30 min with species-matched secondary antibodies conjugated to FITC (ZF-0312) or TRITC (ZF-0316) (1:1000; ZSGB-BIO), then counterstained with DAPI (Beyotime) for nuclear visualization. Slides were mounted using ProLong™ Glass Antifade Mountant (Invitrogen), and images were acquired using a Nikon AXR laser scanning confocal microscope.

Flow cytometry

Jurkat T lymphocytes were subjected to experimental treatments, followed by a 6-h exposure to a cell activation cocktail containing Brefeldin A (BioLegend, 423303) to facilitate intracellular cytokine detection. After fixation and membrane permeabilization, intracellular Granzyme B (GZMB) was stained using an APC-conjugated anti-GZMB monoclonal antibody (BioLegend, 372203). Fluorescence signals were analyzed by flow cytometry, and quantitative data were processed using FlowJo software (v10.8.1).

LDH release assay

WFDC3-knockdown MIA PaCa-2 cells (2×10^3) or WFDC3-overexpressing PANC-1 cells (2×10^3) were co-cultured with Jurkat T cells (1×10^4) in 96-well plates with opaque walls and flat bottoms, using complete tumor cell medium (DMEM), for 48 h at an optimal effector-to-target (E:T) ratio of 5:1. Tumor cells and Jurkat T cells cultured separately served as controls to establish baseline death rates. Cell death was measured using the LDH-Glo™ Cytotoxicity Assay kit (Promega, Catalog No. J2380), and death rates were calculated according to the manufacturer's protocol.

Quantitative real-time PCR (qRT-PCR)

RNA was extracted using the RNA-Quick Purification Kit (Yishan Biotechnology Co., Ltd., cat. RNOOL, Shanghai, China), and reverse transcription into cDNA was carried out with PrimeScript™ RT Master Mix (TaKaRa, Japan) according to the manufacturer's instructions. qRT-PCR was then performed using the QuantiNova SYBR PCR Mix Kit (cat. 4993626, QIAGEN, Germany). GAPDH was used as the endogenous reference gene for normalization. The nucleotide sequences of the amplification primers are listed in Table S1.

Western blot analysis

Cellular lysates were prepared using RIPA buffer supplemented with a protease and phosphatase inhibitor cocktail (Roche Applied Science, Indianapolis, IN, USA). Protein concentrations

were determined using the Pierce BCA Protein Assay Kit (Thermo Fisher Scientific). Proteins were separated by electrophoresis and transferred onto polyvinylidene difluoride (PVDF) membranes (Millipore, Billerica, MA, USA). Membranes were blocked for 1 h at room temperature with 5% nonfat milk, followed by overnight incubation at 4 °C with primary antibodies. The next day, membranes were incubated with secondary antibodies, and signal detection was performed using the ChemiDoc Touch Imaging System (Bio-Rad). GAPDH was used as a loading control. Detailed information on the antibodies used for Western blotting is provided in Table S2. Uncropped Western blot images with clearly labeled molecular weight (kDa) markers are included in the supplementary file.

Statistical analysis

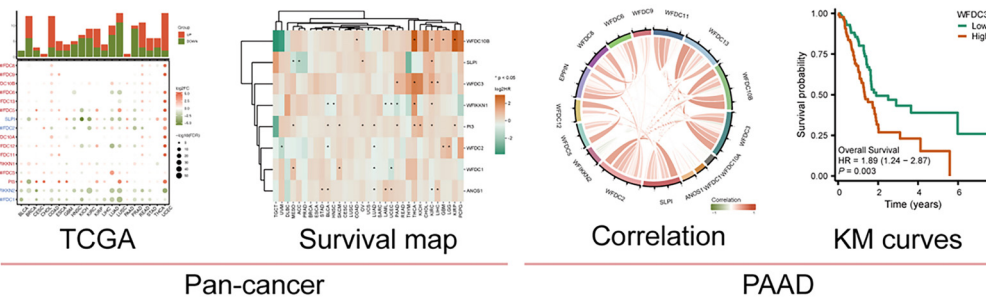
Statistical analyses were conducted using R v4.2.1, Python v3.12.2, ImageJ, and GraphPad Prism v10.2.1. Experimental data from triplicate trials are presented as mean ± SEM. This level of replication was selected in accordance with established standards in molecular biology research to balance statistical rigor with practical constraints on time and resources. Comparisons between two independent groups were assessed using either Student's *t*-test or the Wilcoxon rank-sum test, while multi-group comparisons employed one-way ANOVA followed by Kruskal–Wallis post hoc testing. Survival outcomes, including OS, DSS, and PFI, were evaluated using the Kaplan–Meier method, with survival curves used for graphical representation. For non-normally distributed quantitative variables, correlations were assessed using Pearson's correlation coefficient. Statistical significance was determined using the log-rank test, with a threshold of $P < 0.05$.

Results

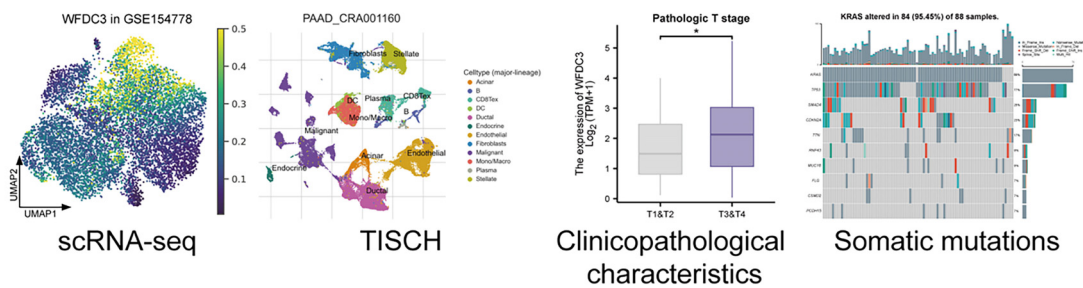
Landscape of WFDC family gene expression and prognostic significance in pan-cancer

A schematic workflow of the experimental procedures is shown in Figure 1. Transcriptional profiles of WFDC genes across malignancies were systematically evaluated through a pan-cancer analysis of TCGA datasets. Distinct expression patterns emerged across cancer types (Figure 2A), with heatmap visualization highlighting pronounced upregulation of WFDC family genes in colon adenocarcinoma (COAD) and uterine corpus endometrial carcinoma (UCEC). In contrast, lung adenocarcinoma (LUAD), lung squamous cell carcinoma (LUSC), and prostate adenocarcinoma (PRAD) exhibited predominant transcriptional suppression. *SLPI*, *WFDC2*, *WFIKKN2*, and *WFDC1* consistently showed low expression across tumor types, whereas *WFDC5*, *WFDC3*, and *WFIKKN1* displayed heterogeneous expression profiles. Univariate Cox regression analysis was used to assess the prognostic relevance of WFDC genes across various cancers (Figure 2B). The resulting survival map revealed significant associations between specific WFDC members and OS in select malignancies. Notably, *WFDC10B*, *WFDC3*, *PI3*, and *ANOS1* were linked to poorer prognosis, as reflected by elevated hazard ratios. Conversely, *SLPI*, *WFIKKN1*, *WFDC2*, and *WFDC1* demonstrated variable prognostic

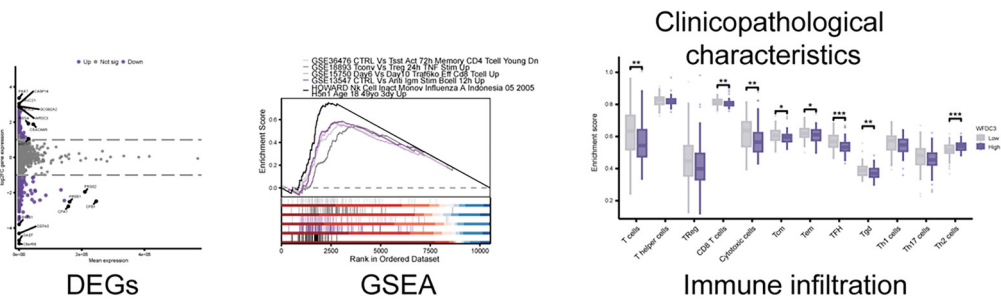
The expression and prognostic values of *WFDC3*



Clinicopathological and mutational analysis of *WFDC3* in PAAD



Functional enrichment and immune infiltration analysis of *WFDC3*



In vitro validation and establishment of the prognostic model

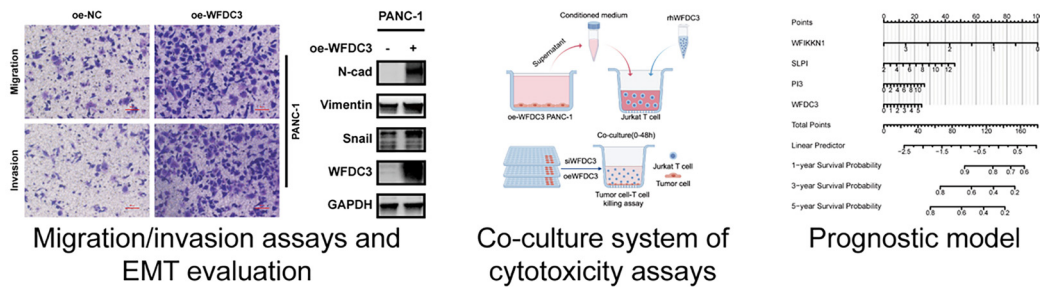


Figure 1. The flowchart of this study. DEG: Differentially expressed gene; EMT: Epithelial–mesenchymal transition; GSEA: Gene Set Enrichment Analysis; scRNA-seq: Single-cell RNA sequencing; WFDC: Whey acidic protein four-disulfide core.

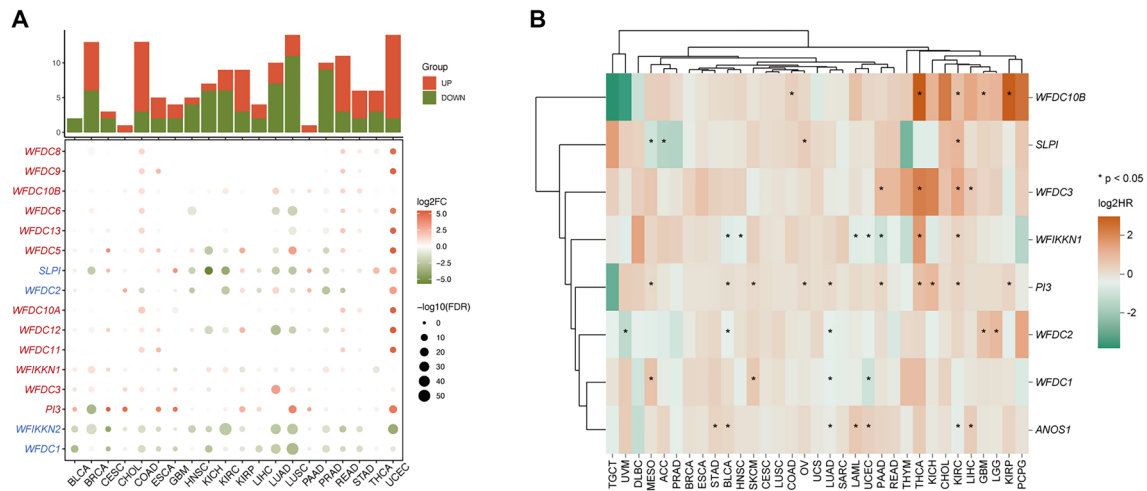


Figure 2. Landscape of WFDC family genes expression and survival in pan-cancer. (A) Bubble heatmap of WFDC family genes expression across tumor types, with the stacked bar chart above visualizing the number of WFDC family genes that are upregulated or downregulated in each cancer type. Genes with elevated expression in most tumors compared to normal tissue are labeled in red, while those with significantly reduced expression are labeled in blue. (B) Survival map based on univariate Cox regression analysis of WFDC family genes for OS across multiple cancers. * $P < 0.05$. FC: Fold change; FDR: False discovery rate; OS: Overall survival; HR: Hazard ratio; WFDC: Whey acidic protein four-disulfide core.

effects across cancer types, suggesting context-dependent, microenvironment-driven functional duality. These trends were further supported by survival validation analyses using the GSCA database (Figure S1A and S1B). Bubble charts illustrated the associations of WFDC gene expression with multiple clinical outcomes, including OS, progression-free survival (PFS), disease-free interval (DFI), and DSS. Stage-specific transcriptional patterns were also characterized (Figure S1C), revealing distinct stage-dependent signatures among WFDCs. Longitudinal analysis of expression trends during tumor progression (Figure S1D) demonstrated dynamic modulation of WFDC gene expression across cancer stages. Collectively, these findings underscore the malignancy-specific transcriptional regulation of the WFDC family and highlight their potential roles in tumor progression and clinical outcomes.

Expression and prognostic value of WFDC family in PAAD

Comparative expression analysis of WFDC genes between PAAD tumors and normal pancreatic tissues was performed using integrated TCGA-GTEx datasets. Visualization of the transcriptional landscape revealed marked differences in WFDC gene expression profiles between malignant and non-malignant samples (Figure 3A). Statistical analysis showed significant tumor-specific upregulation of *WFDC1*, *WFDC2*, *WFDC3*, *SLPI*, *PI3*, and *ANOS1* ($P < 0.0001$), while *WFIKKN1* was notably downregulated in neoplastic tissues ($P < 0.0001$) (Figure 3B). Correlation analysis revealed complex interrelationships among WFDC genes in PAAD, with strongly correlated expression patterns among genes exhibiting similar regulation (Figure 3C). A comprehensive correlation matrix was also constructed to quantify these relationships (Figure S2), identifying several significant associations. Notably, *WFDC3* showed strong positive correlations with multiple family members, suggesting its potential central role in regulating WFDC family functions in PAAD. A detailed survival analysis—encompassing OS, DSS, and PFI—was conducted to assess the prognostic value

of WFDC genes (Figure 3D; Figure S3). Initial OS-related associations were visualized using a heatmap (Figure 3D). *WFDC3* consistently demonstrated prognostic significance across multiple cancers, particularly in PAAD, showing associations with poorer OS, DSS, and PFI outcomes (Figure S4). Elevated *WFDC3* expression was associated with reduced OS (HR = 1.89, 95% CI = 1.24–2.87, $P = 0.003$; Figure 3G), DSS (HR = 2.02, 95% CI = 1.26–3.02, $P = 0.003$; Figure S3A), and PFI (HR = 1.64, 95% CI = 1.11–2.42, $P = 0.014$; Figure S3B). In contrast, *WFIKKN1* expression correlated with improved clinical outcomes. Kaplan-Meier survival curves revealed that higher *WFIKKN1* expression was significantly associated with longer OS (HR = 0.51, 95% CI = 0.32–0.81, $P = 0.004$; Figure 3E), DSS (HR = 0.56, 95% CI = 0.33–0.94, $P = 0.0028$; Figure S3A), and PFI (HR = 0.44, 95% CI = 0.24–0.73, $P = 0.001$; Figure S3B).

WFDC3 correlates with malignant evolution of ductal cells in PAAD

Transcriptional profiling using TCGA datasets revealed elevated *WFDC3* expression in PAAD tumor tissues compared to adjacent or normal pancreatic tissues (Figure S5). scRNA-seq data from TISCH showed that *WFDC3* is predominantly expressed in malignant epithelial cell clusters (Figure S6). The GSE154778 dataset includes scRNA-seq profiles from 10 primary and six metastatic PAAD specimens, summarizing the proportions of five major cell types: epithelial cells, fibroblasts, lymphoid cells, myeloid cells, and plasma cells (Figure 4A). UMAP dimensionality reduction effectively distinguished these cell populations, with epithelial cells forming the largest cluster (Figure 4B). Marker genes for each annotated cluster are shown in Figure S7. Notably, *WFDC3* exhibited strong cell-type specificity, with predominant expression in epithelial cells, as demonstrated by UMAP visualization (Figure 4C). Quantitative analysis confirmed significantly higher *WFDC3*

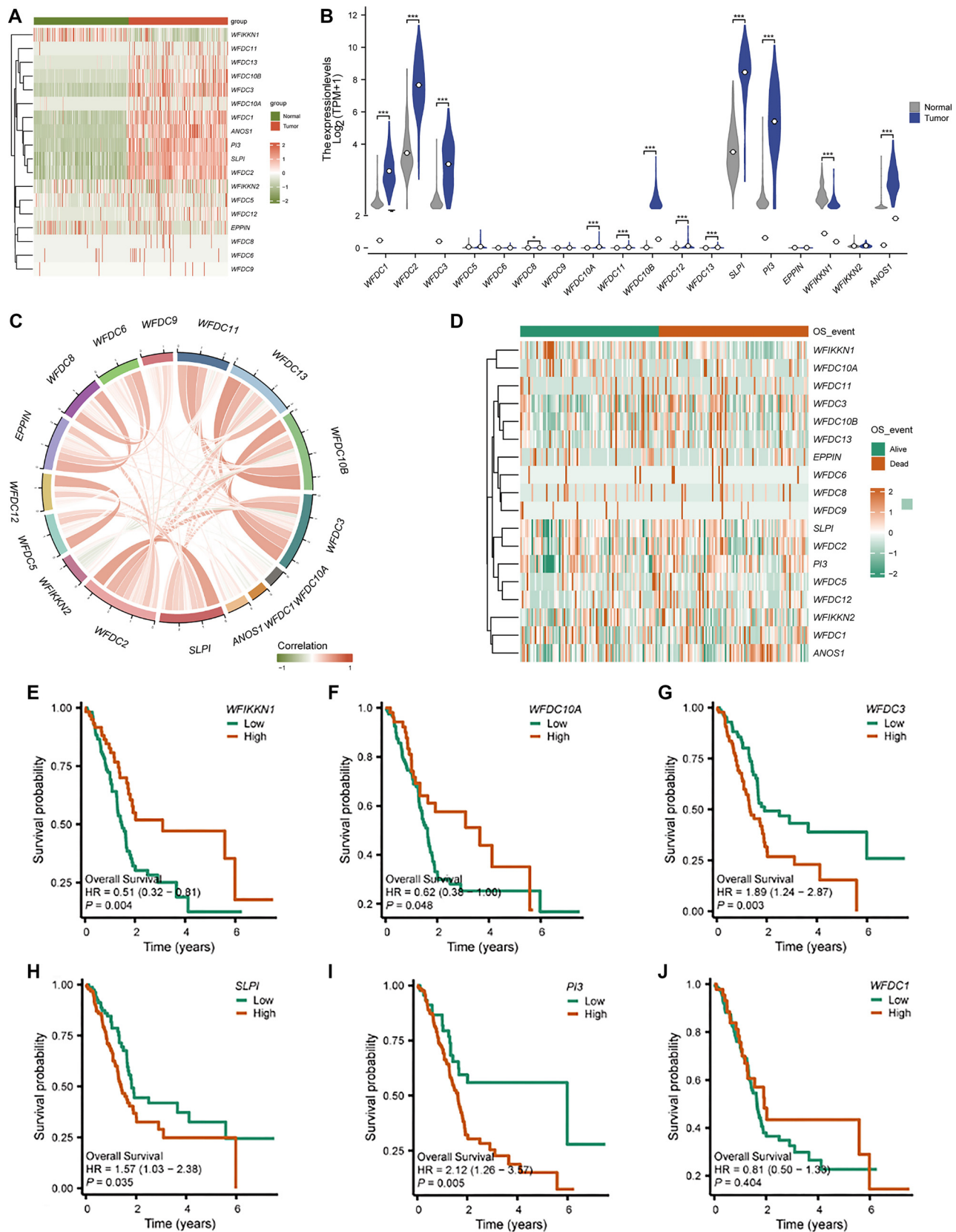


Figure 3. The expression and prognostic value of WFDC family genes in pancreatic cancer. (A) Heatmap and (B) violin plots of the different mRNA expression of WFDC family genes between normal and tumor tissues in PAAD based on the TCGA and the GTEx datasets; (C) Chord diagram of Pearson correlations among WFDC family genes in PAAD; (D) Heatmap of WFDC family gene expression based on OS events; (E–J) KM curves of OS between patients with high and low WFDC family genes expression level. * $P < 0.05$, *** $P < 0.001$. OS: Overall survival; HR: Hazard ratio; KM: Kaplan–Meier; WFDC: Whey acidic protein four-disulfide core.

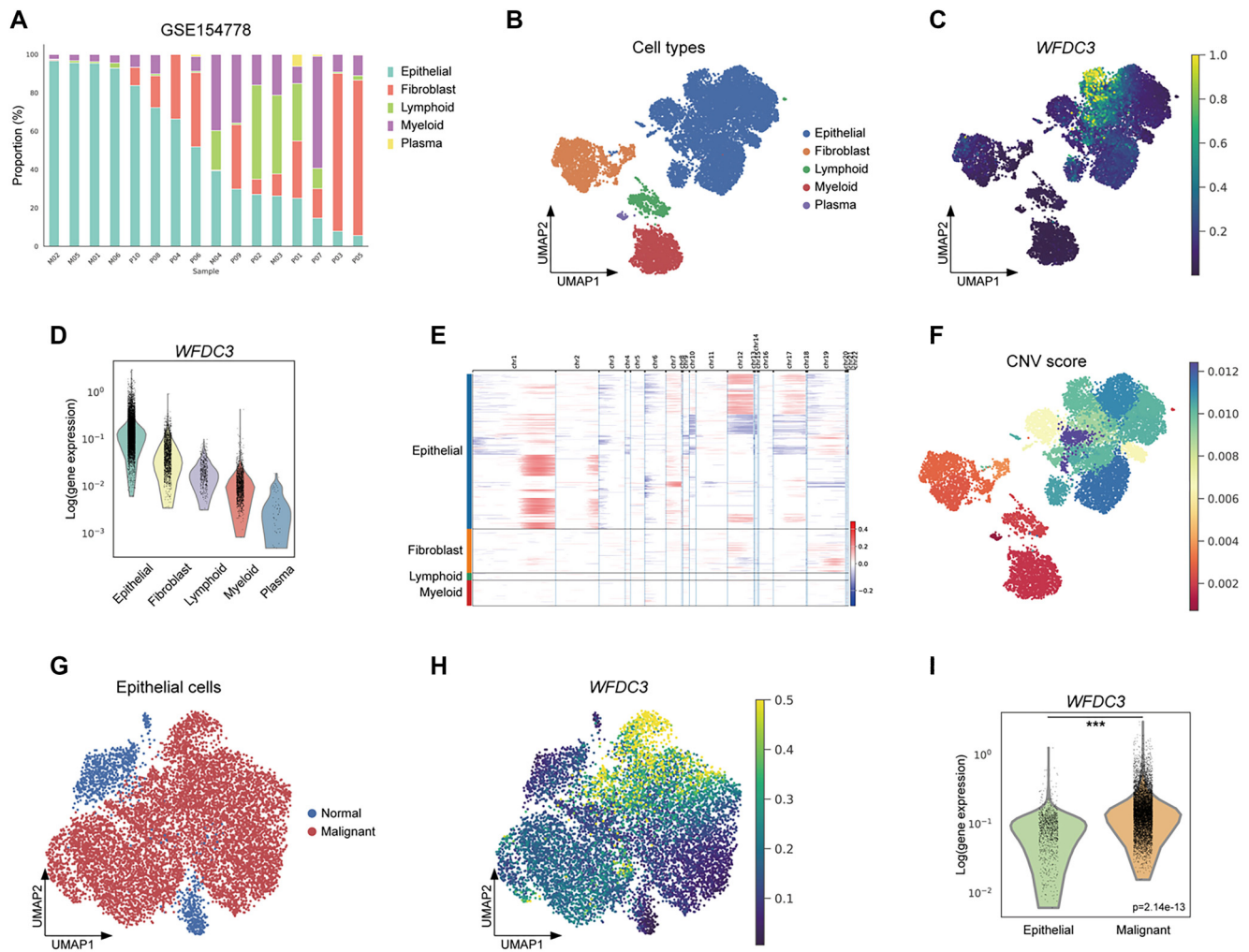


Figure 4. *WFDC3* exhibited specific expression in malignant epithelial cells of PAAD. (A) The GSE154778 dataset comprises scRNA-seq data from 10 primary and six metastatic PAAD specimens, with cellular composition summarized across five major categories: Epithelial, fibroblast, lymphoid, myeloid, and plasma cells; (B) Major cell type distribution was visualized through UMAP dimensionality reduction; (C) Transcriptional profiles of *WFDC3* across all cellular subsets; (D) Violin plots depicted normalized *WFDC3* expression intensities within the five principal cell lineages; (E) InferCNV analysis was implemented using stromal cells as a reference population; (F) CNV scores were projected onto UMAP coordinates for spatial resolution; (G) Malignant epithelial cells were distinguished from normal counterparts based on elevated chromosomal instability; (H) UMAP visualization and (I) violin plots compared *WFDC3* expression between malignant and non-malignant epithelial populations. Statistical significance was assessed via Mann–Whitney *U* testing (* $P < 0.05$, ** $P < 0.01$, *** $P < 0.0001$). scRNA-seq: Single-cell RNA sequencing; WFDC: Whey Acidic protein four-disulfide core.

expression in epithelial cells compared to fibroblasts, lymphoid cells, myeloid cells, and plasma cells (Figure 4D). InferCNV analysis, using stromal cells as a reference, revealed distinct chromosomal copy number variations (Figure 4E), which were mapped onto the UMAP to visualize CNV scores (Figure 4F). This approach enabled identification of malignant epithelial cells based on chromosomal instability patterns. Subsequent stratification of epithelial cells into normal and malignant subsets (Figure 4G) enabled detailed evaluation of *WFDC3* expression. UMAP visualization (Figure 4H) and statistical analysis (Figure 4I) showed significantly elevated *WFDC3* expression in malignant vs normal epithelial cells ($P = 2.14 \times 10^{-13}$). Additional scRNA-seq analysis from our unpublished independent dataset further examined the cellular distribution and potential role of *WFDC3* in tumor progression. UMAP plots identified distinct cell populations (Figure S8A), with *WFDC3* expression mapped

across them (Figure S8B). Detailed analysis indicated predominant *WFDC3* expression in ductal cells (Figure S8C), with significantly higher expression in IPMN and PDAC ductal cells compared to normal uninvolved (UNIN) ductal cells (Figure S8D and S8E, *** $P < 0.001$), supporting a role for *WFDC3* in the malignant transformation of ductal cells in PAAD. Clinicopathological correlations of *WFDC3* expression in PAAD were evaluated systematically (Figure S9A). Advanced T-stage tumors (T3&T4) exhibited significantly higher *WFDC3* expression than early-stage tumors (T1&T2; $P < 0.05$). Similarly, patients with residual tumors (R1&R2) had elevated *WFDC3* levels compared to those with complete resections (R0; $P < 0.05$). Although N1-stage tumors showed a trend toward increased *WFDC3* expression relative to N0-stage, this difference was not statistically significant. Genomic mutation analysis from the TCGA-PAAD cohort revealed distinct mutational landscapes between high

and low *WFDC3* expression groups (Figure S9B and S9C). In the high-expression group, *KRAS* mutations were detected in 84 of 88 samples (95.45%), frequently accompanied by alterations in *TP53* (77%), *SMAD4* (25%), and *CDKN2A* (23%). Additional but less frequent mutations included *TTN* (17%), *RNF43* (9%), and *MUC16* (9%). The low-expression group also had *KRAS* as the most frequently mutated gene, though at a lower frequency (76.25%; 61 of 80 samples). This group maintained a similar driver gene profile with *TP53* (50%), *SMAD4* (22%), and *CDKN2A* (11%), albeit at reduced frequencies. These differences suggest potential molecular mechanisms linking *WFDC3* expression to pancreatic tumorigenesis and progression.

Functional enrichment analysis of *WFDC3* related DEGs in PAAD

To elucidate *WFDC3*'s molecular mechanisms, systematic transcriptome profiling was performed. Comparative analysis between *WFDC3*-high and -low expression cohorts identified 3100 DEGs, including 820 upregulated and 2280 downregulated transcripts. An MA plot (Figure 5A) highlighted notable upregulation of *PAX7*, *CASPI4*, and *MUC21*, alongside significant downregulation of *PRSS1*, *PRSS2*, *CPBI*, and *DEFA5*. GO analysis of upregulated DEGs revealed significant enrichment ($P < 0.05$) in biological processes, such as epidermal morphogenesis, protease activity modulation, and immune regulation (Figure 5B). Cellular component analysis indicated enrichment in intermediate filament networks, while molecular function analysis pointed to signaling receptor activation and transcriptional regulation. KEGG pathway analysis identified upregulation in estrogen signaling and *Staphylococcus aureus* infection pathways. In contrast, downregulated DEGs were enriched in pathways related to transmembrane potential homeostasis, hormonal regulation, and immune modulation (Figure 5C). These genes were associated with synaptic structures and ion channel complexes at the cellular level, and predominantly involved in transmembrane transport and receptor activities at the functional level. KEGG analysis further indicated significant downregulation in pancreatic secretion, insulin secretion, and protein digestion pathways. GSEA identified ten significantly altered pathways ($FDR < 0.001$) (Figure 5D). Among these, *MYC* targets V1 ($NES = 2.907$), G2M checkpoint ($NES = 2.886$), and E2F targets ($NES = 2.870$) showed strong positive enrichment, whereas the pancreatic beta cell pathway exhibited pronounced negative enrichment ($NES = -2.575$). Additional enrichment was observed in interferon alpha response, hypoxia, and the p53 pathway, indicating involvement of complex regulatory networks. Further GSEA (Figure 5E and 5F) uncovered distinct immunological signatures and metabolic alterations, suggesting comprehensive reprogramming of the immune microenvironment in response to *WFDC3* expression levels.

Relationship between *WFDC3* expression and tumor-infiltrating immune cells in PAAD

Association studies between *WFDC3* expression and immune cell subsets across various malignancies revealed complex immunomodulatory networks (Figure S10). CIBERSORT deconvolution analysis identified distinct correlations between *WFDC3* levels and immune cell infiltration in PAAD (Figure 6A).

Among these, M0 macrophages exhibited the strongest positive correlation ($R = 0.388$, $P < 0.001$), followed by memory B cells ($R = 0.243$, $P < 0.01$) and regulatory T cells (Tregs; $R = 0.183$, $P < 0.05$). In contrast, naïve B cells showed the most pronounced negative correlation ($R = -0.318$, $P < 0.001$), with $CD8^+$ T lymphocytes ($R = -0.281$, $P < 0.001$) and plasma cells ($R = -0.241$, $P < 0.01$) also inversely associated with *WFDC3* expression. ESTIMATE-based computational analysis revealed significant differences in tumor microenvironment parameters between high and low *WFDC3* expression groups (Figure 6B). Stromal ($P < 0.05$), immune ($P < 0.05$), and composite ESTIMATE scores ($P < 0.05$) all varied significantly, underscoring *WFDC3*'s impact on the tumor microenvironment architecture. ssGSEA-based quantification of T cell subtypes further showed that *WFDC3*-high tumors had reduced infiltration of total T cells ($P < 0.01$), $CD8^+$ T cells ($P < 0.01$), and cytotoxic subsets ($P < 0.01$) (Figure 6C). Decreased infiltration was also observed in central memory (Tcm), effector memory (Tem), follicular helper (TFH), and $\gamma\delta$ T cells (Tgd). Notably, T helper 2 cells (Th2) were paradoxically elevated in *WFDC3*-high tumors ($P < 0.001$), emphasizing the multifaceted immunoregulatory role of *WFDC3* in the pancreatic tumor microenvironment. Together, these findings suggest that *WFDC3* significantly influences the immune landscape in PAAD, potentially promoting immune evasion and tumor progression through modulation of specific immune cell populations.

WFDC3 promoted PAAD cell migration and invasion *in vitro*

Transcriptomic profiling revealed elevated *WFDC3* expression in PAAD, prompting investigation into its regulatory mechanisms. Protein-level validation of *WFDC3* expression was performed across normal pancreatic epithelial HPNE cells and several PAAD cell lines (MIA PaCa-2, PANC-1, AsPC-1, and BxPC-3) (Figure S11A). Comparative analysis confirmed consistent *WFDC3* upregulation in malignant cell lines relative to HPNE controls, with the highest expression observed in MIA PaCa-2 and BxPC-3 cells. Gain-of-function studies were conducted by plasmid-mediated *WFDC3* overexpression in PANC-1 cells, with successful transcriptional and translational upregulation confirmed by qRT-PCR (Figure S11B) and ELISA (Figure S11C). Cell proliferation dynamics were assessed using CCK-8 assays, colony formation assays, and EdU incorporation analyses. Longitudinal CCK-8 assays revealed no significant difference in viability between *WFDC3*-overexpressing and control cells (Figure S11D). This lack of proliferative effect was corroborated by comparable colony-forming abilities (Figure S11E) and similar proportions of EdU-positive cells (Figure S11F). Our previous studies demonstrated *WFDC3*-mediated suppression of epithelial-mesenchymal transition (EMT) in CRC [16]. In contrast, current findings indicate that *WFDC3* promotes PAAD cell migration and invasion through EMT modulation (Figure 7). Transwell assays showed significantly increased migration and invasion in *WFDC3*-overexpressing PANC-1 cells (Figure 7A), while *WFDC3* knockdown in MIA PaCa-2 cells reduced these capabilities (Figure 7B). These results establish *WFDC3* as a facilitator of PAAD cell motility and invasiveness. To elucidate the underlying mechanisms, EMT marker

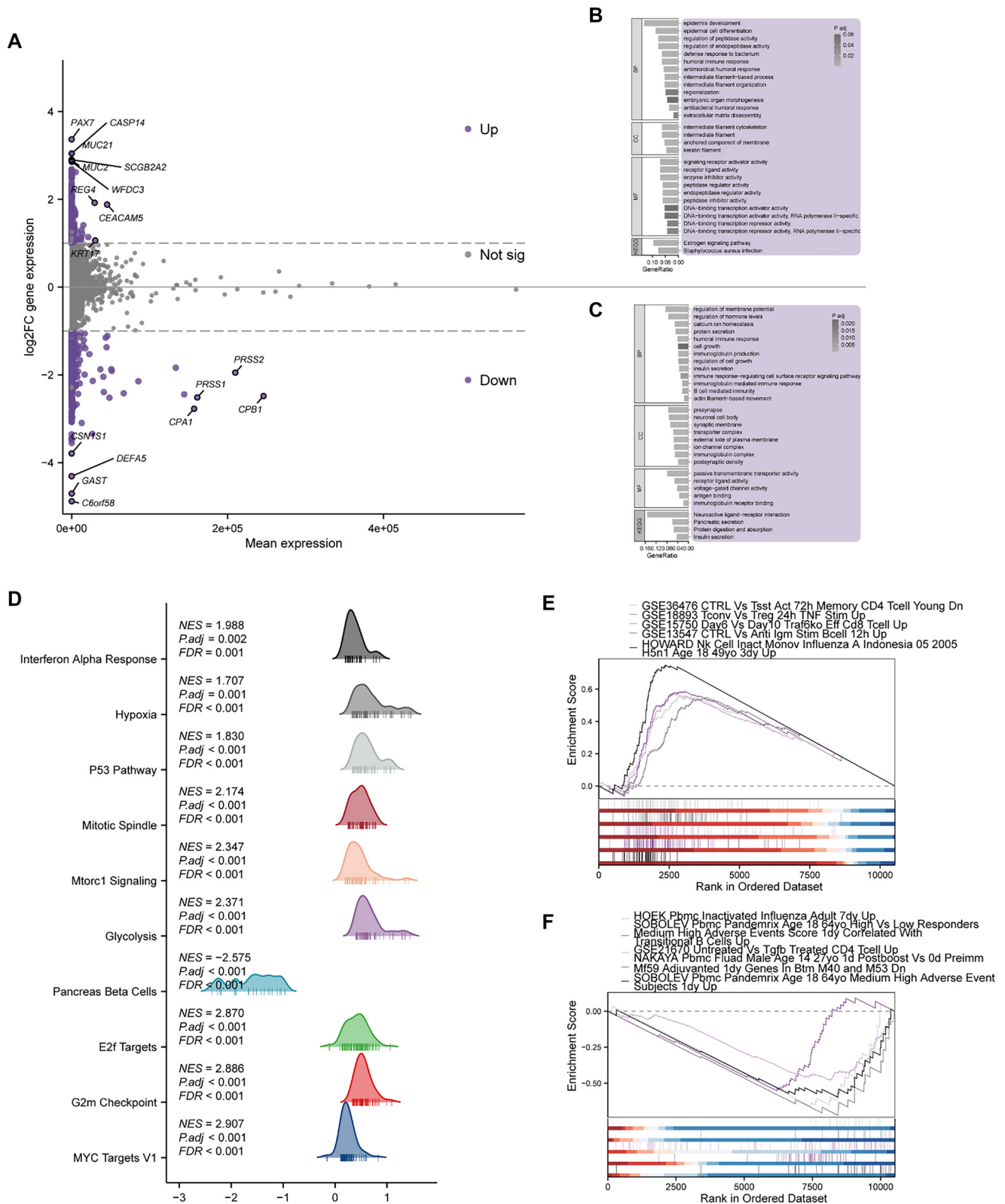


Figure 5. Transcriptional landscape and pathway modulation across *WFDC3* expression strata. (A) MA (M-vs-A) plot demonstrated genome-wide differential expression patterns; (B) Functional categorization of upregulated transcriptional variants in *WFDC3*-high cohorts through GO and KEGG pathway enrichment; (C) GO/KEGG profiling of downregulated genes in *WFDC3*-elevated specimens; (D–F) Gene set enrichment profiling (GSEA) of transcriptional variants across expression clusters. GSEA: Gene Set Enrichment Analysis; *WFDC3*: Whey acidic protein four-disulfide core; KEGG: Kyoto Encyclopedia of Genes and Genomes; GO: Gene Ontology.

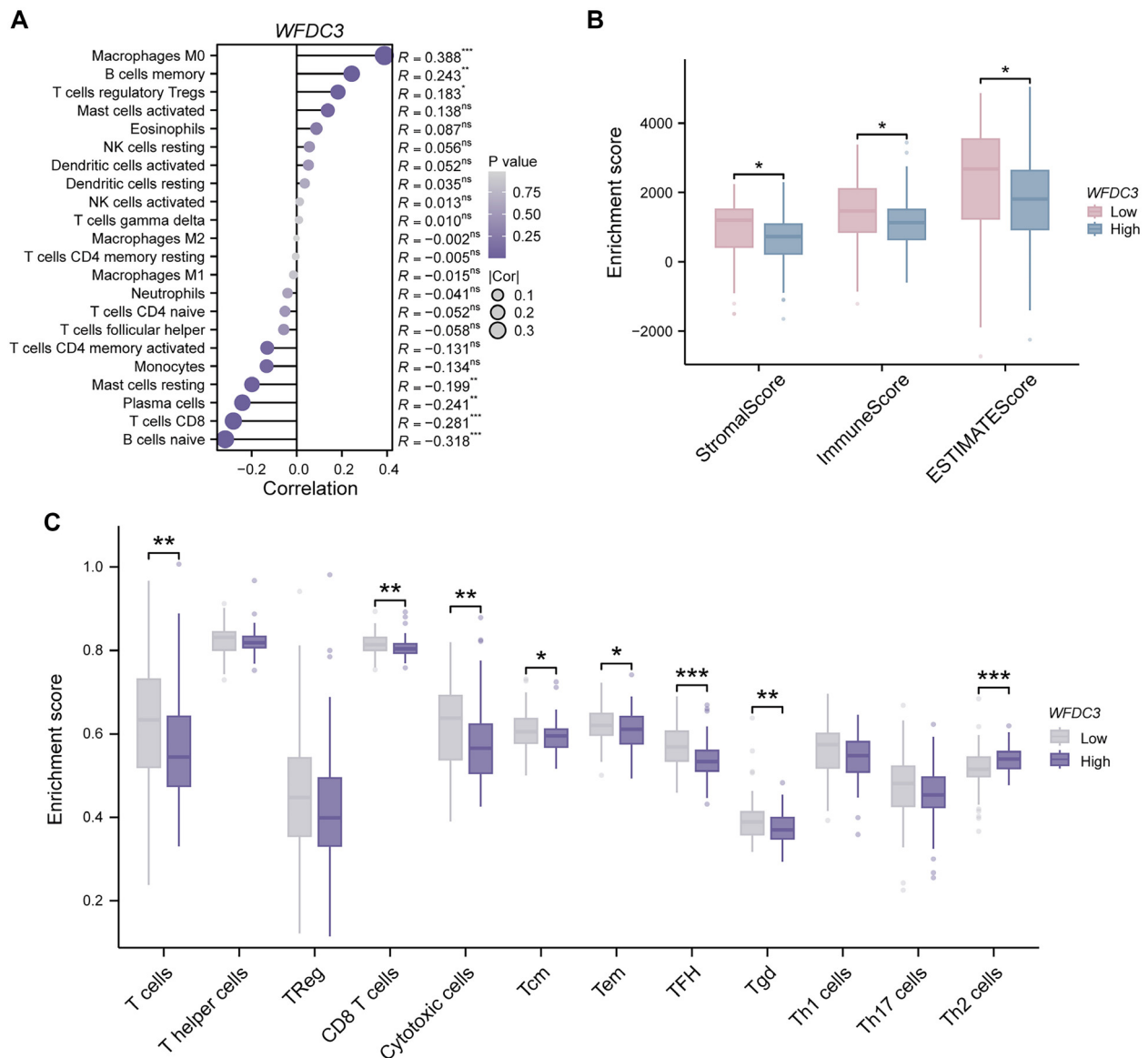


Figure 6. Immune microenvironment characterization associated with *WFDC3* expression in TCGA-PAAD cohort. (A) Immune infiltration patterns associated with *WFDC3* expression in PAAD were evaluated using CIBERSORT methodology; (B) Comparative assessment of stromal components, immune infiltration metrics, and composite ESTIMATE scores between *WFDC3* expression cohorts was performed via the ESTIMATE algorithm; (C) Quantitative profiling of principal T lymphocyte subsets across *WFDC3* expression strata was conducted through ssGSEA-based computational analysis. * $P < 0.05$, ** $P < 0.01$, *** $P < 0.001$. GSEA: Gene Set Enrichment Analysis; WFDC: Whey acidic protein four-disulfide core.

expression was analyzed. Overexpression of *WFDC3* in PANC-1 cells led to increased levels of mesenchymal markers, including N-cadherin, Vimentin, and Snail (Figure 7C), indicative of EMT induction. This was further supported by IF staining, which showed decreased expression of the tight junction protein ZO-1 and increased N-cadherin levels in *WFDC3*-overexpressing cells (Figure 7E). Conversely, *WFDC3* knockdown in MIA PaCa-2 cells led to upregulation of the epithelial marker E-cadherin and downregulation of mesenchymal markers Vimentin and Snail (Figure 7D). Additionally, ZO-1 and E-cadherin expression were elevated following *WFDC3* knockdown (Figure 7F). In summary, *WFDC3* facilitates PAAD progression by enhancing migration and invasion through EMT induction. These findings position *WFDC3* as a key regulator of pancreatic cancer

aggressiveness and highlight its potential as a therapeutic target for metastasis suppression in PAAD.

WFDC3 inhibited T cell cytotoxicity in PAAD

Functional enrichment analysis provided evidence that *WFDC3* exerts systemic immunosuppressive effects on T cells. To further evaluate its impact on T cell cytotoxicity, multiple experimental approaches were employed (Figure 8A and 8B). Flow cytometry revealed that treatment with recombinant human *WFDC3* (rh*WFDC3*, 10 ng/mL) significantly reduced GZMB expression in Jurkat T cells compared to the vehicle control ($P < 0.01$) (Figure 8C and 8D). Similarly, conditioned medium from *WFDC3*-overexpressing PANC-1 cells (oe*WFDC3*-CM) markedly decreased the proportion

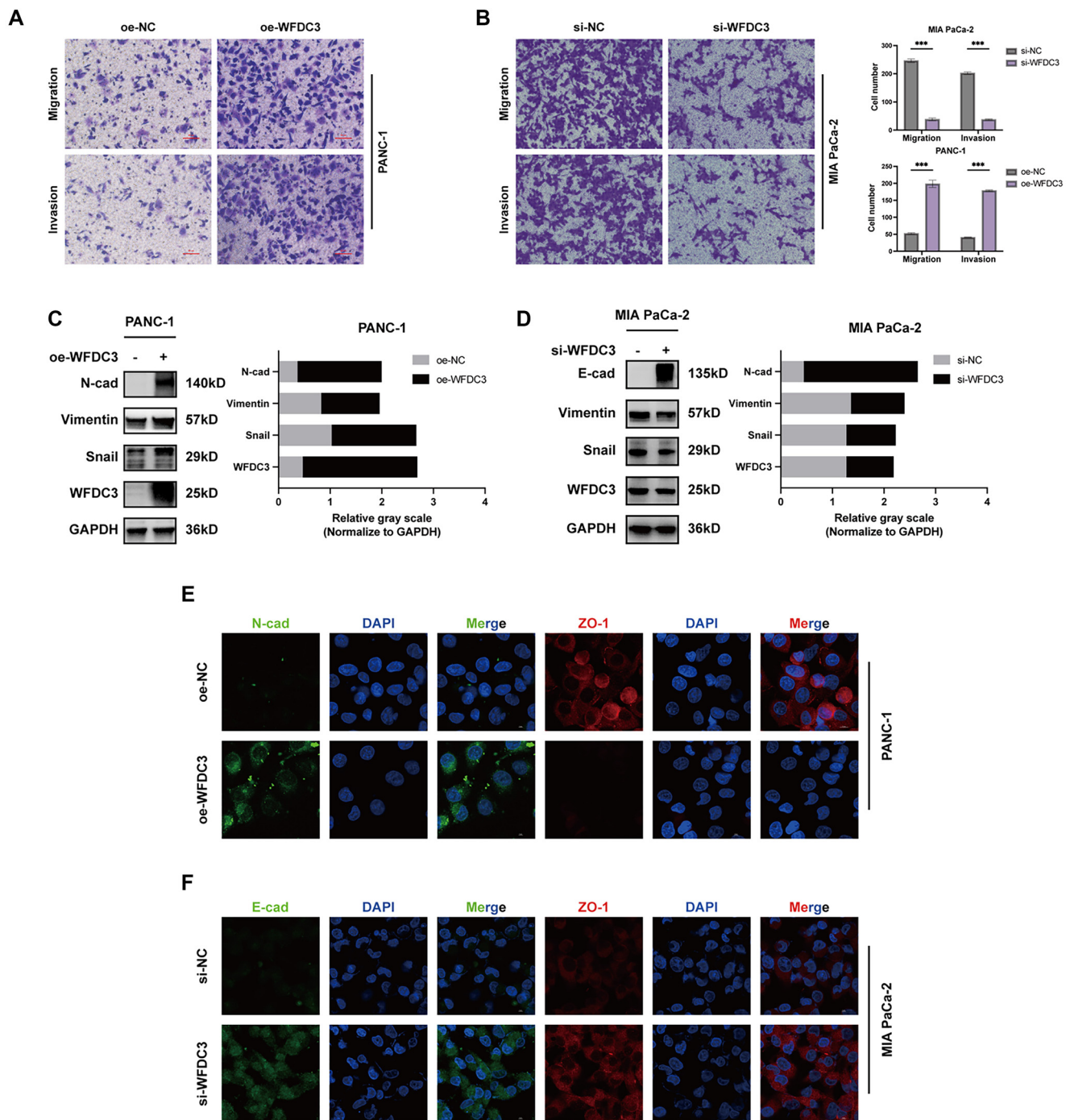


Figure 7. WFDC3 promoted PAAD cell migration and invasion *in vitro*. Transwell assays were used to evaluate the migration and invasion capacity of WFDC3 overexpression in PANC-1 (A) and WFDC3 knockdown in MIA PaCa-2 (B), scale bar: 50µm. (C and D) Western blot together with gray values and (E and F) Immunofluorescence staining was used to detect the expression of EMT related proteins, scale bar: 5µm. ****P* < 0.001. EMT: Epithelial-mesenchymal transition; WFDC: Whey acidic protein four-disulfide core.

of GZMB-positive Jurkat T cells relative to that cultured in normal control medium (NC-CM) (Figure 8E and 8F). Molecular analyses corroborated these findings, showing broad suppression of T cell cytotoxic function. qRT-PCR demonstrated that under WFDC3-overexpressing conditions, the expression of key cytotoxic mediators—including IFNG, IL2, Perforin, GZMB, and Granulysin (GNLY)—was

significantly reduced (*P* < 0.05) (Figure 8G), with similar expression patterns observed following rhWFDC3 treatment (Figure 8H). Furthermore, co-culture experiments provided strong support for WFDC3's immunosuppressive role. Co-culturing Jurkat T cells with WFDC3-knockdown MIA PaCa-2 cells enhanced T cell-mediated killing, as evidenced by decreased cell viability in CCK-8 assays (Figure 8I) and

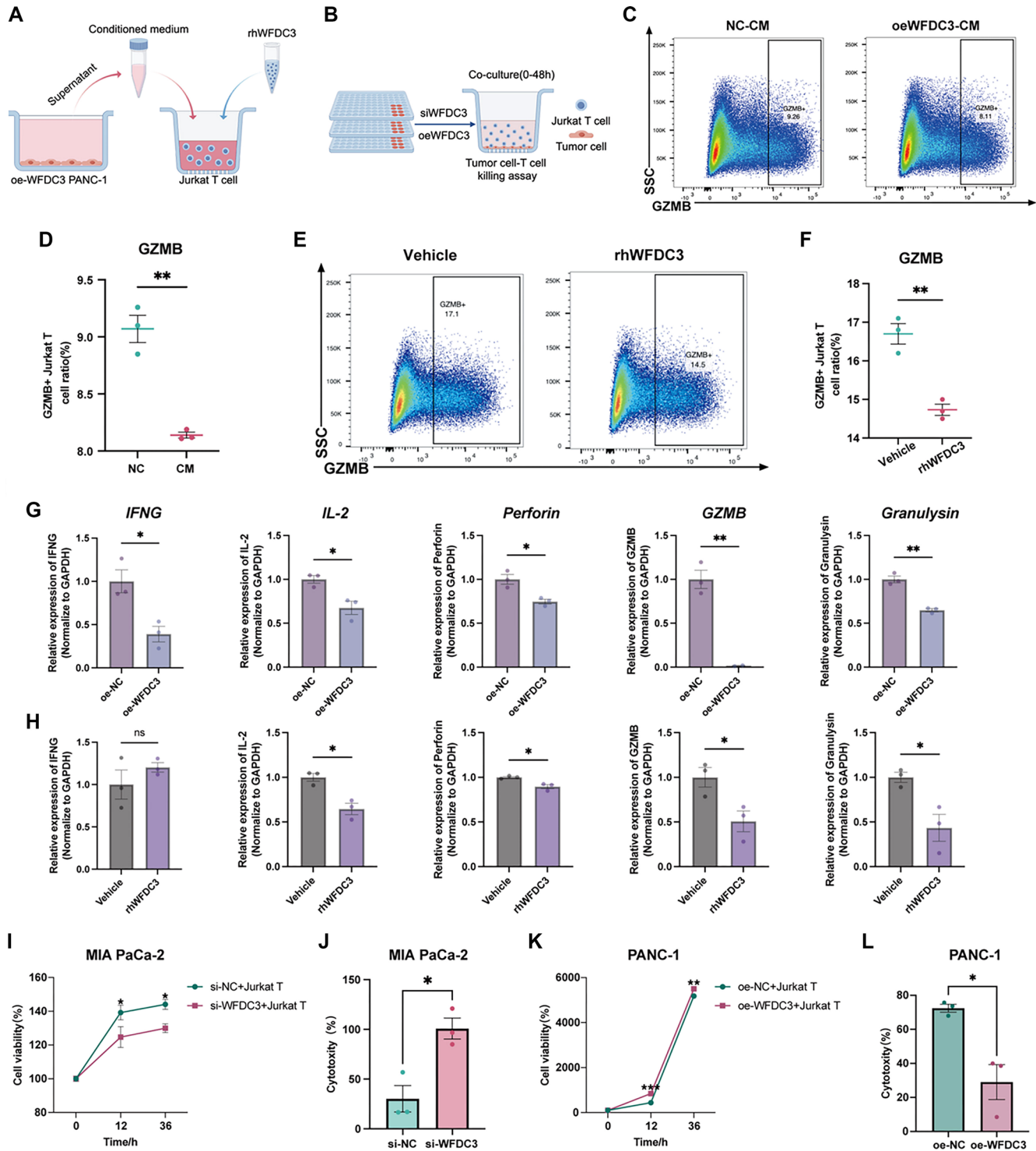


Figure 8. WfDC3 inhibited T cell cytotoxicity in PAAD. (A and B) Schematic representation of the experimental design by Figdraw. (C and D) Levels of GZMB in Jurkat T cells treated with conditional medium collected from WFDC3 overexpressed PANC-1 cells was assessed via flow cytometric analysis. (E and F) Levels of GZMB in Jurkat T cells treated with rhWFDC3 (10 ng/mL) was assessed via flow cytometric analysis. qRT-PCR was performed to evaluate T cell cytotoxicity-related markers using RNA retracted from PANC-1 cells after (G) transfected with WFDC3 overexpression plasmid or (H) treated with rhWFDC3 (10 ng/mL). (I) CCK-8 assay and (J) LDH release assay was performed in WFDC3-knockdown MIA PaCa-2 cells cocultured with Jurkat T cells to evaluate T cell cytotoxicity. (K) CCK-8 assay and (L) LDH release assay was performed in WFDC3-overexpression PANC-1 cells cocultured with Jurkat T cells. * $P < 0.05$, ** $P < 0.01$, *** $P < 0.001$. WFDC: Whey acidic protein four-disulfide core; GZMB: Granzyme B; qRT-PCR: Quantitative real-time PCR.

increased cytotoxicity in LDH release assays (Figure 8J). Conversely, PANC-1 cells overexpressing WFDC3 were more resistant to T cell-mediated killing, maintaining higher viability (Figure 8K) and exhibiting significantly reduced LDH release ($P < 0.05$) (Figure 8L). Collectively, these findings indicate that WFDC3 acts as a potent immunosuppressive factor in pancreatic cancer, impairing T cell cytotoxicity through both direct suppression of cytotoxic effector expression and reduced susceptibility to T cell-mediated cell killing.

Establishment and validation of the prognostic model based on WFDCs

A prognostic model for PAAD based on WFDC family genes was developed and validated using the TCGA-PAAD cohort. LASSO regression analysis of 18 WFDC genes identified four key genes—WFDC3, WFIKKN1, PI3, and SLPI—that were significantly associated with OS (Figure 9A). Univariate Cox regression confirmed the prognostic relevance of these biomarkers: WFIKKN1 was associated with a protective effect (HR < 1, $P < 0.001$), while WFDC3, PI3, and SLPI were linked to worse outcomes (HR > 1, $P > 0.05$) (Figure 9B). A multivariable risk model was constructed using the formula: Risk score = $0.068 \times \text{WFDC3} + (-0.5398) \times \text{WFIKKN1} + 0.041 \times \text{PI3} + 0.0738 \times \text{SLPI}$. Patients were stratified into high- and low-risk groups based on the median risk score. Multimodal visualizations, including scatter plots and heatmaps, illustrated clear associations between gene expression patterns and survival, with elevated mortality observed in the high-risk group (Figure 9C). Kaplan–Meier survival curves confirmed a significant difference in OS between risk groups, with higher mortality in the high-risk cohort ($P = 0.00144$) (Figure 9D). Model performance was evaluated via time-dependent ROC analysis, yielding AUC values of 0.62 (one-year), 0.695 (three-year), and 0.837 (five-year), supporting the model's predictive validity (Figure 9E). A multivariate nomogram incorporating the four-gene signature was created to estimate one-, three-, and five-year survival probabilities, providing a practical tool for individualized risk assessment (Figure 9F). Calibration curves showed strong agreement between predicted and observed outcomes across all time points, underscoring the model's accuracy (Figure 9G). Correlation analysis between risk scores and immune infiltration revealed significant associations with various immune cell types, including macrophages and T-cell subsets, suggesting the model reflects key interactions between tumor progression and the immune microenvironment (Figure 9H). To validate the model externally, two independent PAAD cohorts from the GEO database (GSE62452 and GSE78229) were analyzed. Patient risk scores were calculated using the established formula, and stratification by median values effectively divided them into high- and low-risk groups. Kaplan–Meier analysis confirmed significantly better survival in the low-risk groups across both datasets ($P < 0.05$, Figure 9I and 9J), reinforcing the model's generalizability and prognostic utility. These findings support the use of the four-gene WFDCs-based signature for risk stratification and potentially guiding immunotherapeutic strategies in PAAD.

Discussion

The WFDC family members are multifaceted contributors to oncological processes, modulating inflammation, immune regulation, cell adhesion, signaling pathways, and extracellular matrix remodeling. Collectively, these functions promote tumorigenesis and disease progression, positioning the WFDC family as a critical research frontier in cancer biology [25, 26]. Although functional conservation exists among family members, notable differences in expression patterns and mechanisms are observed. For example, WFDC1 is downregulated in the stroma of prostate tumors, regulates the COX-2 pathway, and mediates immune cell interactions—suggesting a tumor-suppressive role [27–30]. In contrast, WFDC4 promotes metastasis in ovarian cancer via PI3K-AKT pathway activation and MMP-9 secretion [31]. WFDC2, one of the most extensively studied members, displays a functional dichotomy: it serves as a diagnostic biomarker in lung, ovarian, and prostate cancers [11, 15, 32, 33], with clinical utility as a serum marker for ovarian cancer [34], yet paradoxically suppresses prostate cancer metastasis by inhibiting EGFR-mediated cell migration [15]. These context-dependent roles highlight the need for systematic pan-cancer studies to clarify the tissue-specific oncogenic and tumor-suppressive functions of WFDC proteins. To explore the regulatory mechanisms of WFDC family members across cancers, a comprehensive analytical framework was developed. Pan-cancer transcriptional profiling revealed heterogeneous WFDCs expression, indicative of functional plasticity dependent on tumor context. Univariate Cox survival modeling identified significant correlations between WFDCs expression and OS in multiple cancers, with high expression levels often associated with poorer prognosis. PAAD, the third leading cause of cancer-related death globally, exhibits a 10% five-year survival rate and a median survival of less than six months [2, 35]. Limited treatment options, resistance to therapy, and a lack of effective biomarkers contribute to its poor prognosis, underscoring the urgent need for novel therapeutic strategies [1]. However, the role of WFDC proteins in PAAD remains largely unexplored. To address this gap, we conducted an in-depth analysis of WFDC family members in PAAD using integrated TCGA and GTEx datasets. This enabled a comparison of mRNA expression between tumor and adjacent normal tissues, revealing that more than half of the WFDC genes were transcriptionally upregulated in tumors. These findings were validated across datasets, indicating conserved expression patterns. Correlation analyses—employing two complementary methods—revealed strong co-expression among WFDC members, suggesting potential synergistic roles in PAAD biology. Subsequent survival analyses identified WFDC3 and WFIKKN1 as both prognostic biomarkers and potential functional contributors to PAAD progression. Their consistent association with patient outcomes across multiple survival metrics underscores their clinical relevance. Furthermore, univariate Cox regression followed by LASSO modeling identified four key prognostic WFDC members (WFDC3, WFIKKN1, SLPI, and PI3). The resulting predictive model demonstrated strong performance in forecasting PAAD patient outcomes, supporting the translational potential of WFDCs-based prognostic tools.

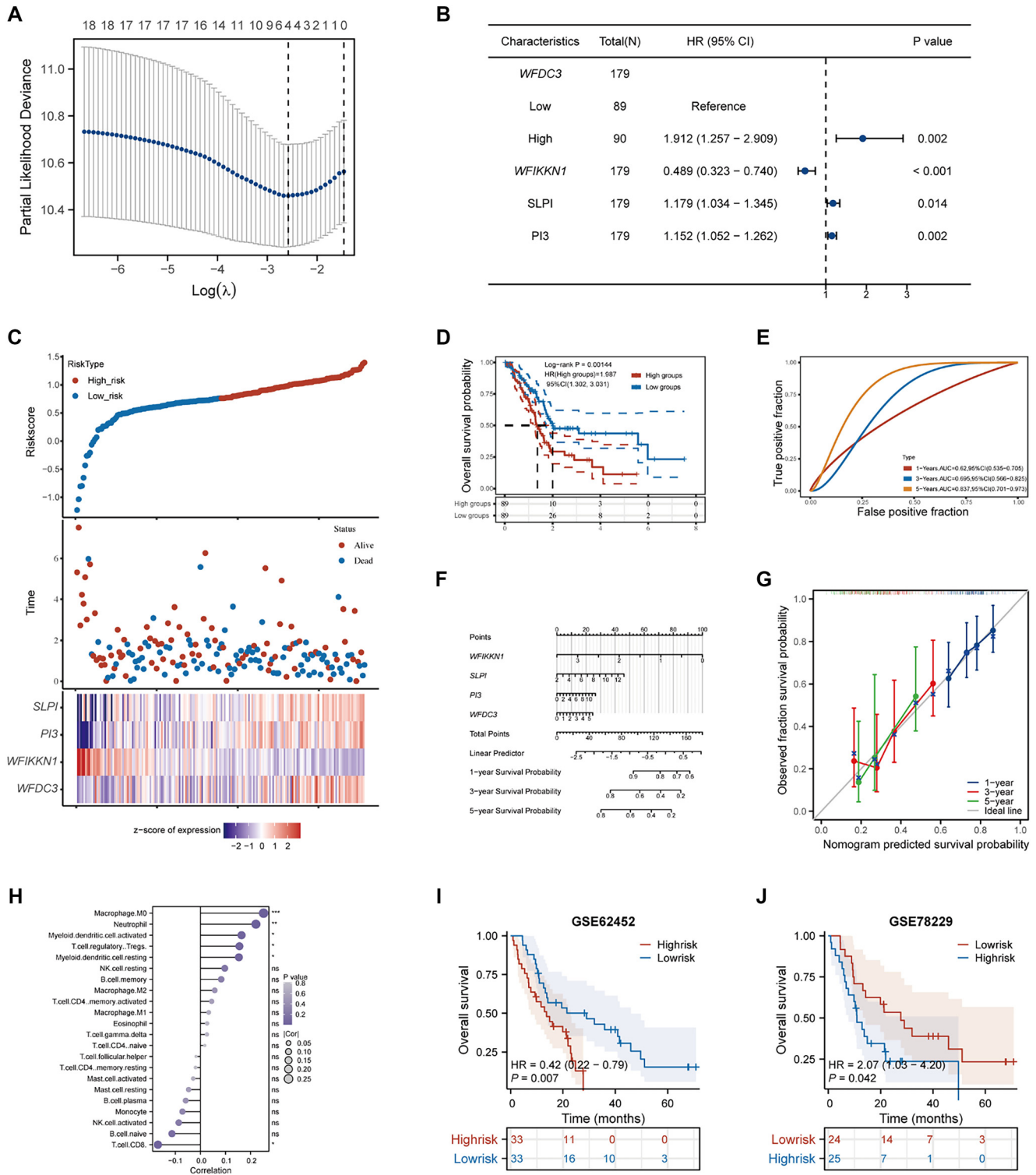


Figure 9. Prognostic risk model derivation utilizing WFDC family genes in TCGA-PAAD cohort. (A) LASSO regression analysis of 18 WFDC family members; (B) Univariate Cox regression forest plot identifying four OS-associated WFDC genes; (C) Patient stratification via median risk score thresholding (upper), with survival status distribution (middle) and four-gene expression patterns (lower) visualized; (D) Kaplan–Meier survival curves comparing high- vs low-risk cohorts; (E) ROC curve validation of risk score predictive accuracy; (F) Multivariate nomogram for pancreatic cancer survival probability estimation; (G) Calibration curves evaluating one-/three-/five-year OS prediction concordance; (H) Immune cell correlation profiling with risk model parameters. (I and J) The Kaplan–Meier analysis of the external validation cohorts. * $P < 0.05$, ** $P < 0.01$, *** $P < 0.001$. WFDC: Whey acidic protein four-disulfide core; OS: Overall survival.

Current research on *WFDC3* remains limited. A recent study investigating the functional roles of *WFDC* genes in various aspects of male fertility reported that *WFDC3* knockout mice did not exhibit any apparent reproductive defects [36]. Additionally, multi-omic analyses of PAAD conducted by Cao et al. [37] revealed upregulation of *WFDC3* at the transcriptomic level. In the present study, *WFDC3* was found to be significantly upregulated in PAAD and associated with poor prognosis—a finding that contrasts with previous reports of its tumor-suppressive role in CRC [16]. These results suggest that *WFDC3* may exhibit complex, tissue-specific functions in the development of PAAD. Consistent with bulk RNA sequencing data, scRNA-seq analysis provided critical insights into the cellular distribution of *WFDC3*, confirming its predominant expression in malignant epithelial cells. Furthermore, a progressive increase in *WFDC3* mRNA levels from UNIN to IPMN to PDAC suggests its potential involvement in the malignant transformation of pancreatic ductal cells. This finding is particularly relevant given the ongoing challenges in elucidating the molecular mechanisms underlying PAAD oncogenesis. The principal oncogenic drivers in PAAD pathogenesis include *KRAS*, *CDKN2A*, *TP53*, and *SMAD4*. While *KRAS* and *CDKN2A* mutations typically arise during tumor initiation, aberrations in *TP53* and *SMAD4* are associated with disease progression and malignant transformation [38]. Our analysis revealed a correlation between *WFDC3* expression and mutations in these driver genes, with notably higher *KRAS* mutation frequencies observed in *WFDC3*-high cohorts. Clinically, advanced-stage PAAD patients exhibited significantly elevated *WFDC3* expression compared to early-stage patients. These findings support the role of *WFDC3* as a tumor-promoting factor and an independent adverse prognostic biomarker in PAAD. To elucidate the functional implications of *WFDC3*, we performed enrichment analyses on DEGs between *WFDC3*-high and -low expression groups. GO and KEGG pathway analyses revealed marked enrichment in cytoskeletal reorganization processes, particularly intermediate filament assembly and actin-mediated motility, indicating a potential role for *WFDC3* in modulating cellular structural plasticity. Substantial evidence links dynamic cytoskeletal remodeling to tumor metastasis [39, 40], suggesting that *WFDC3* may contribute to metastatic progression by influencing cytoskeletal dynamics. In addition, functional annotations highlighted significant involvement in immune regulatory pathways, including humoral immunity, B cell activation, and immunoglobulin-mediated responses. GSEA corroborated these findings and uncovered further associations with cell cycle regulation, notably G2/M checkpoint control and mitotic spindle organization. Immune-related pathways were particularly enriched, with the interferon-alpha response prominently represented. Further GSEA analyses revealed strong associations with T cell inhibition and broader modulation of immune responses. Enrichment scores varied notably across different immune cell states, underscoring *WFDC3*'s role in fine-tuning specific immune functions. These molecular insights highlight the dual regulatory role of *WFDC3* in cytoskeletal organization and immune response modulation. The enriched pathways align with prior observations linking

WFDC3 to tumor progression and survival, suggesting it may influence PAAD development through coordinated regulation of cell motility and immune dynamics.

Immune-checkpoint inhibitors (ICIs) have revolutionized cancer therapeutics through their novel mechanism of action [41, 42]. These agents enhance tumor targeting by promoting immune recognition of tumor-specific neoantigens, which are processed into immunogenic peptides that activate cytotoxic CD8⁺ T lymphocytes capable of eliminating malignant cells [43]. However, PAAD exhibits intrinsic resistance to ICIs, primarily due to two factors: a relatively low neoantigen burden compared to other malignancies and the presence of a complex, immunosuppressive TME. Together, these factors impair T cell activation and dampen antitumor immune responses [44–47]. Developing innovative strategies to overcome these immunosuppressive mechanisms remains an urgent research priority. PAAD is characterized by a highly reactive and desmoplastic stroma [48]. Investigating the interaction between cancer cells with upregulated *WFDC3* and other cellular components of the tumor immune microenvironment may yield novel insights into therapeutic strategies targeting *WFDC3*-mediated immune regulation. Our analysis revealed a negative association between *WFDC3* expression and multiple immune cell populations, suggesting broad immunosuppressive effects. Subsequent ESTIMATE analysis demonstrated that high *WFDC3* expression correlated with significantly lower ImmuneScore, StromaScore, and ESTIMATEScore, indicating reduced immune cell infiltration in the tumor stroma and impaired antitumor immune responses. Notably, *WFDC3* showed a strong negative correlation with various T cell subsets. Further analysis confirmed that elevated *WFDC3* expression was significantly associated with reduced infiltration and activity of multiple functional T cell subtypes, including cytotoxic T cells, CD8⁺ T cells, and T follicular helper cells—populations essential for sustaining antitumor immunity [49]. These findings suggest that *WFDC3* may contribute to immune evasion by suppressing T cell-mediated immune responses. Given its immunosuppressive role and negative association with T cell infiltration, we hypothesized that *WFDC3* expression might influence response to immunotherapy. However, due to the limited availability of immunotherapy-treated PAAD cohorts, we utilized a CRC immunotherapy dataset (GSE53127) for preliminary evaluation [50, 51]. The analysis revealed significantly higher *WFDC3* expression in responders compared to non-responders (Figure S12). This observation aligns with previous findings identifying *WFDC3* as a tumor suppressor in CRC and supports its potential role as a context-dependent modulator of immune sensitivity [16]. These findings underscore the need for further investigation into the predictive value of *WFDC3* in immunotherapy-treated cohorts, particularly in immune-refractory malignancies such as PAAD.

Building on previous research [16, 17] and the bioinformatic findings presented above, we hypothesized that *WFDC3* functions as a dispensable regulator within the molecular modulation network of pancreatic cancer—a notion further substantiated by *in vitro* experiments. Elevated *WFDC3* protein expression in pancreatic cancer cells was confirmed via

Western blot analysis. Notably, gain- and loss-of-function experiments revealed that WFDC3 does not influence cell proliferation. This finding partially contradicts earlier reports, potentially due to the complex regulatory mechanisms in physiological environments, where multiple signaling pathways and cellular interactions collectively fine-tune WFDC3's functional output. Nonetheless, we observed that WFDC3 promote PAAD cell migration and invasion through EMT induction, consistent with our analyses. The conserved structural domains of the WFDC family confer intrinsic protease inhibitory activity [52, 53], and growing interest surrounds their potential role in tumor immune regulation [54]. SLPI, for instance, has been shown to mediate its antiprotease-related immunoregulatory effects through various mechanisms [55, 56]. This study provides the first experimental evidence that WFDC3 exerts an immunosuppressive effect by attenuating T cell cytotoxicity, although the precise regulatory mechanisms remain unclear and warrant further investigation. While this study offers novel insights into the prognostic relevance of WFDC3 in PAAD, several methodological limitations should be acknowledged. The use of publicly available datasets introduces potential selection bias, underscoring the need for validation in independent, large-scale PAAD cohorts with detailed clinicopathological annotations. Moreover, the clinical utility of WFDC3 as a biomarker, along with our prognostic model, requires thorough evaluation. Although *in vitro* experiments confirmed WFDC3's pro-metastatic and immunosuppressive properties, systematic *in vivo* studies are essential to uncover the underlying mechanisms and assess the therapeutic potential of targeting WFDC3 in immunotherapy-resistant PAAD patients.

Conclusion

In conclusion, our pan-cancer analytical framework revealed distinct expression patterns of the WFDC family and identified WFDC3 as a promising prognostic biomarker and therapeutic target in PAAD, owing to its dual association with metastatic progression and modulation of the immune microenvironment. This study highlights WFDC3's critical regulatory role in PAAD pathogenesis and underscores the need for further mechanistic investigations to clarify its specific oncogenic pathways.

Conflicts of interest: Authors declare no conflicts of interest.

Funding: This work was funded by: National High Level Hospital Clinical Research Funding (2022-PUMCH-B-063); Chinese Academy of Medical Sciences (CAMS) Innovation Fund for Medical Sciences (CIFMS) (2021-I2M-1-002); the Fundamental Research Funds for the Central Universities (3332024008).

Data availability: The data supporting the findings of this study are available from the corresponding authors upon reasonable request.

Submitted: 22 March 2025

Accepted: 17 April 2025

Published online: 08 May 2025

Liu et al.

WFDC3 as biomarker in pancreatic cancer

References

- [1] Park W, Chawla A, O'Reilly EM. Pancreatic cancer: a review. *JAMA* 2021;326:851. <https://doi.org/10.1001/jama.2021.13027>.
- [2] Siegel RL, Giaquinto AN, Jemal A. Cancer statistics, 2024. *CA Cancer J Clin* 2024;74:12–49. <https://doi.org/10.3322/caac.21820>.
- [3] Han B, Zheng R, Zeng H, Wang S, Sun K, Chen R, et al. Cancer incidence and mortality in China, 2022. *J Natl Cancer Cent* 2024;4:47–53. <https://doi.org/10.1016/j.jncc.2024.01.006>.
- [4] Hu ZI, O'Reilly EM. Therapeutic developments in pancreatic cancer. *Nat Rev Gastroenterol Hepatol* 2024;21:7–24. <https://doi.org/10.1038/s41575-023-00840-w>.
- [5] von Ahrens D, Bhagat TD, Nagrath D, Maitra A, Verma A. The role of stromal cancer-associated fibroblasts in pancreatic cancer. *J Hematol Oncol* 2017;10:76. <https://doi.org/10.1186/s13045-017-0448-5>.
- [6] Clauss A, Lilja H, Lundwall A. A locus on human chromosome 20 contains several genes expressing protease inhibitor domains with homology to whey acidic protein. *Biochem J* 2002;368:233–42. <https://doi.org/10.1042/BJ20020869>.
- [7] Ranganathan S, Simpson KJ, Shaw DC, Nicholas KR. The whey acidic protein family: a new signature motif and three-dimensional structure by comparative modeling. *J Mol Graph Model* 1999;17:106–13, 134–6. [https://doi.org/10.1016/s1093-3263\(99\)00023-6](https://doi.org/10.1016/s1093-3263(99)00023-6).
- [8] Bingle C. Towards defining the complement of mammalian WFDC-domain-containing proteins. *Biochem Soc Trans* 2011;39:1393–7. <https://doi.org/10.1042/BST0391393>.
- [9] Bingle CD, Vyakarnam A. Novel innate immune functions of the whey acidic protein family. *Trends Immunol* 2008;29:444–53. <https://doi.org/10.1016/j.it.2008.07.001>.
- [10] Larsen M, Ressler SJ, Gerdes MJ, Lu B, Byron M, Lawrence JB, et al. The WFDC1 gene encoding ps20 localizes to 16q24, a region of LOH in multiple cancers. *Mamm Genome Off J Int Mamm Genome Soc* 2000;11:767–73. <https://doi.org/10.1007/s003350010135>.
- [11] Bingle L, Cross SS, High AS, Wallace WA, Rassl D, Yuan G, et al. WFDC2 (HE4): a potential role in the innate immunity of the oral cavity and respiratory tract and the development of adenocarcinomas of the lung. *Respir Res* 2006;7:61. <https://doi.org/10.1186/1465-9921-7-61>.
- [12] Scott A, Weldon S, Taggart CC. SLPI and elafin: multifunctional antiproteases of the WFDC family. *Biochem Soc Trans* 2011;39:1437–40. <https://doi.org/10.1042/BST0391437>.
- [13] Zhong H, Qian Y, Fang S, Yang L, Li L, Gu W. HE4 expression in lung cancer, a meta-analysis. *Clin Chim Acta Int J Clin Chem* 2017;470:109–14. <https://doi.org/10.1016/j.cca.2017.05.007>.
- [14] Han C, Bellone S, Siegel ER, Altwerger G, Menderes G, Bonazzoli E, et al. A novel multiple biomarker panel for the early detection of high-grade serous ovarian carcinoma. *Gynecol Oncol* 2018;149:585–91. <https://doi.org/10.1016/j.ygyno.2018.03.050>.
- [15] Xiong Y, Yuan L, Chen S, Xu H, Peng T, Ju L, et al. WFDC2 suppresses prostate cancer metastasis by modulating EGFR signaling inactivation. *Cell Death Dis* 2020;11:537. <https://doi.org/10.1038/s41419-020-02752-y>.
- [16] Liu T, Zhao M, Peng L, Chen J, Xing P, Gao P, et al. WFDC3 inhibits tumor metastasis by promoting the ERβ-mediated transcriptional repression of TGFBR1 in colorectal cancer. *Cell Death Dis* 2023;14:425. <https://doi.org/10.1038/s41419-023-05956-0>.
- [17] Yang X, Weng K, Xing P, Chen J, Hao H, Liu T, et al. WFDC3 sensitizes colorectal cancer to chemotherapy by regulating ATM/ATR kinase signaling pathway. *FASEB J* 39;2:e70329. <https://doi.org/10.1096/fj.202402472R>.
- [18] Wolf FA, Angerer P, Theis FJ. SCANPY: large-scale single-cell gene expression data analysis. *Genome Biol* 2018;19:15. <https://doi.org/10.1186/s13059-017-1382-0>.
- [19] Gayoso A, Lopez R, Xing G, Boyeau P, Valiollah Pour Amiri V, Hong J, et al. A python library for probabilistic analysis of single-cell omics data. *Nat Biotechnol* 2022;40:163–6. <https://doi.org/10.1038/s41587-021-01206-w>.
- [20] Virshup I, Bredikhin D, Heumos L, Palla G, Sturm G, Gayoso A, et al. The scverse project provides a computational ecosystem for single-cell omics data analysis. *Nat Biotechnol* 2023;41:604–6. <https://doi.org/10.1038/s41587-023-01733-8>.
- [21] Chen B, Khodadoust MS, Liu CL, Newman AM, Alizadeh AA. Profiling tumor infiltrating immune cells with CIBERSORT. *Methods Mol Biol* 2018;1711:243–59. https://doi.org/10.1007/978-1-4939-7493-1/_12.
- [22] Yoshihara K, Shahmoradgoli M, Martínez E, Vegesna R, Kim H, Torres-García W, et al. Inferring tumour purity and stromal and immune cell

- admixture from expression data. *Nat Commun* 2013;4:2612. <https://doi.org/10.1038/ncomms3612>.
- [23] Hänzelmann S, Castelo R, Guinney J. GSEA: gene set variation analysis for microarray and RNA-seq data. *BMC Bioinformatics* 2013;14:7. <https://doi.org/10.1186/1471-2105-14-7>.
- [24] Bindea G, Mlecnik B, Tosolini M, Kirilovsky A, Waldner M, Obenauf AC, et al. Spatiotemporal dynamics of intratumoral immune cells reveal the immune landscape in human cancer. *Immunity* 2013;39:782–95. <https://doi.org/10.1016/j.immuni.2013.10.003>.
- [25] Bouchard D, Morisset D, Bourbonnais Y, Tremblay GM. Proteins with whey-acidic-protein motifs and cancer. *Lancet Oncol* 2006;7:167–74. [https://doi.org/10.1016/S1470-2045\(06\)70579-4](https://doi.org/10.1016/S1470-2045(06)70579-4).
- [26] Wen Y, Jiang N, Wang Z, Xiao Y. Versatile whey acidic protein four-disulfide core domain proteins: biology and role in diseases. *Front Cell Dev Biol* 2024;12:1459129. <https://doi.org/10.3389/fcell.2024.1459129>.
- [27] Hickman OJ, Smith RA, Dasgupta P, Rao SN, Nayak S, Sreenivasan S, et al. Expression of two WFDC1/ps20 isoforms in prostate stromal cells induces paracrine apoptosis through regulation of PTGS2/COX-2. *Br J Cancer* 2016;114:1235–42. <https://doi.org/10.1038/bjc.2016.91>.
- [28] Hickman O, Galustian C, Elhage O, Smith RA, Ukimura O, Gill I, et al. 328 Ps20 inhibits expansion of Cd8-t cells and nk cells in the prostate cancer microenvironment and inhibits killing of prostate cancer cells. *J Urol* 2012;187:e133. <https://doi.org/10.1016/j.juro.2012.02.388>.
- [29] Watson JEV, Kamkar S, James K, Kowbel D, Andaya A, Paris PL, et al. Molecular analysis of WFDC1/ps20 gene in prostate cancer. *Prostate* 2004;61:192–9. <https://doi.org/10.1002/pros.20100>.
- [30] Zhu S, Ye L, Bennett S, Xu H, He D, Xu J. Molecular structure, gene expression and functional role of WFDC1 in angiogenesis and cancer. *Cell Biochem Funct* 2021;39:588–95. <https://doi.org/10.1002/cbf.3624>.
- [31] Sun L, Ke M, Wang X, Yin M, Wei J, Xu L, et al. FAPhigh α -SMA^{low} cancer-associated fibroblast-derived SLPI protein encapsulated in extracellular vesicles promotes ovarian cancer development via activation of PI3K/AKT and downstream signaling pathways. *Mol Carcinog* 2022;61:910–23. <https://doi.org/10.1002/mc.23445>.
- [32] James NE, Chichester C, Ribeiro JR. Beyond the biomarker: understanding the diverse roles of human epididymis protein 4 in the pathogenesis of epithelial ovarian cancer. *Front Oncol* 2018;8:124. <https://doi.org/10.3389/fonc.2018.00124>.
- [33] Nagy B, Bhattoa HP, Steiber Z, Csobán M, Szilasi M, Méhes G, et al. Serum human epididymis protein 4 (HE4) as a tumor marker in men with lung cancer. *Clin Chem Lab Med* 2014;52:1639–48. <https://doi.org/10.1515/oclm-2014-0041>.
- [34] Bates M, Mohamed BM, Lewis F, O'Toole S, O'Leary JJ. Biomarkers in high grade serous ovarian cancer. *Biochim Biophys Acta Rev Cancer* 2024;1879:189224. <https://doi.org/10.1016/j.bbcan.2024.189224>.
- [35] Sung H, Ferlay J, Siegel RL, Laversanne M, Soerjomataram I, Jemal A, et al. Global cancer statistics 2020: GLOBOCAN estimates of incidence and mortality worldwide for 36 cancers in 185 countries. *CA Cancer J Clin* 2021;71:209–49. <https://doi.org/10.3322/caac.21660>.
- [36] Kent K, Nozawa K, Parkes R, Dean L, Daniel F, Leng M, et al. Large-scale CRISPR/Cas9 deletions within the WFDC gene cluster uncover gene functionality and critical roles in mammalian reproduction. *Proc Natl Acad Sci* 2024;121:e2413195121. <https://doi.org/10.1073/pnas.2413195121>.
- [37] Cao L, Huang C, Cui Zhou D, Hu Y, Lih TM, Savage SR, et al. Proteogenomic characterization of pancreatic ductal adenocarcinoma. *Cell* 2021;184:5031–52.e26. <https://doi.org/10.1016/j.cell.2021.08.023>.
- [38] Hayashi A, Hong J, Iacobuzio-Donahue CA. The pancreatic cancer genome revisited. *Nat Rev Gastroenterol Hepatol* 2021;18:469–81. <https://doi.org/10.1038/s41575-021-00463-z>.
- [39] Li X, Wang J. Mechanical tumor microenvironment and transduction: cytoskeleton mediates cancer cell invasion and metastasis. *Int J Biol Sci* 2020;16:2014–28. <https://doi.org/10.7150/ijbs.44943>.
- [40] Yu H, Liu L, Hao S. The significance of cytoskeleton system in tumor cell infiltration. *J Adv Med Sci* 2021;4:51. <https://doi.org/10.30564/jams.v4i2.3342>.
- [41] Yu JX, Hubbard-Lucey VM, Tang J. Immuno-oncology drug development goes global. *Nat Rev Drug Discov* 2019;18:899–900. <https://doi.org/10.1038/d41573-019-00167-9>.
- [42] Miguel M de, Calvo E. Clinical challenges of immune checkpoint inhibitors. *Cancer Cell* 2020;38:326–33. <https://doi.org/10.1016/j.ccell.2020.07.004>.
- [43] Schumacher TN, Schreiber RD. Neoantigens in cancer immunotherapy. *Science* 2015;348:69–74. <https://doi.org/10.1126/science.aaa4971>.
- [44] Ullman NA, Burchard PR, Dunne RF, Linehan DC. Immunologic strategies in pancreatic cancer: making cold tumors hot. *J Clin Oncol* 2022;40:2789–805. <https://doi.org/10.1200/JCO.21.02616>.
- [45] Yarchoan M, Johnson BA, Lutz ER, Laheru DA, Jaffee EM. Targeting neoantigens to augment antitumor immunity. *Nat Rev Cancer* 2017;17:209–22. <https://doi.org/10.1038/nrc.2016.154>.
- [46] Balachandran VP, Łuksza M, Zhao JN, Makarov V, Moral JA, Remark R, et al. Identification of unique neoantigen qualities in long-term survivors of pancreatic cancer. *Nature* 2017;551:512–6. <https://doi.org/10.1038/nature24462>.
- [47] Balli D, Rech AJ, Stanger BZ, Vonderheide RH. Immune cytolytic activity stratifies molecular subsets of human pancreatic cancer. *Clin Cancer Res Off J Am Assoc Cancer Res* 2017;23:3129–38. <https://doi.org/10.1158/1078-0432.CCR-16-2128>.
- [48] Ho WJ, Jaffee EM, Zheng L. The tumour microenvironment in pancreatic cancer—clinical challenges and opportunities. *Nat Rev Clin Oncol* 2020;17:527–40. <https://doi.org/10.1038/s41571-020-0363-5>.
- [49] Steele NG, Carpenter ES, Kemp SB, Sirihorachai VR, The S, Delrosario L, et al. Multimodal mapping of the tumor and peripheral blood immune landscape in human pancreatic cancer. *Nat Cancer* 2020;1:1097–112. <https://doi.org/10.1038/s43018-020-00121-4>.
- [50] Pentheroudakis G, Kotoula V, Fountzilias E, Kouvatsos G, Basdanis G, Xanthakis I, et al. A study of gene expression markers for predictive significance for bevacizumab benefit in patients with metastatic colon cancer: a translational research study of the hellenic cooperative oncology group (HeCOG). *BMC Cancer* 2014;14:111. <https://doi.org/10.1186/1471-2407-14-111>.
- [51] Ding T, Shang Z, Zhao H, Song R, Xiong J, He C, et al. Anoikis-related gene signatures in colorectal cancer: implications for cell differentiation, immune infiltration, and prognostic prediction. *Sci Rep* 2024;14:11525. <https://doi.org/10.1038/s41598-024-62370-y>.
- [52] Lundwall Å, Clauss A. Genes encoding WFDC- and kunitz-type protease inhibitor domains: are they related? *Biochem Soc Trans* 2011;39:1398–402. <https://doi.org/10.1042/BST0391398>.
- [53] Silva AAS, Raimundo TRF, Mariani NAP, Kushima H, Avellar MCW, Buffone MG, et al. Dissecting EPPIN protease inhibitor domains in sperm motility and fertilizing ability: repercussions for male contraceptive development. *Mol Hum Reprod* 2021;27:gaab066. <https://doi.org/10.1093/molehr/gaab066>.
- [54] Eatemadi A, Aiyelabegan HT, Negahdari B, Mazlomi MA, Daraee H, Daraee N, et al. Role of protease and protease inhibitors in cancer pathogenesis and treatment. *Biomed Pharmacother* 2017;86:221–31. <https://doi.org/10.1016/j.biopha.2016.12.021>.
- [55] Cui C, Chakraborty K, Tang XA, Zhou G, Schoenfelt KQ, Becker KM, et al. Neutrophil elastase selectively kills cancer cells and attenuates tumorigenesis. *Cell* 2021;184:3163–77.e21. <https://doi.org/10.1016/j.cell.2021.04.016>.
- [56] Balood M, Ahmadi M, Eichwald T, Ahmadi A, Majdoubi A, Roversi K, et al. Nociceptor neurons affect cancer immunosurveillance. *Nature* 2022;611:405–12. <https://doi.org/10.1038/s41586-022-05374-w>.

Related articles

1. The prognostic value of MKL1 in predicting breast cancer immune infiltrates and chemosensitivity
Yijia Hua and Mengzhu Yang, BJBMS, 2021
2. CLEC11A expression as a prognostic biomarker in correlation to immune cells of gastric cancer
Weidan Fang et al., Biomol Biomed, 2023
3. Cyclin B1: A potential prognostic and immunological biomarker in pan-cancer
Quan Chen et al., Biomol Biomed, 2024
4. CTHRC1 is associated with *BRAF*(V600E) mutation and correlates with prognosis, immune cell infiltration, and drug resistance in colon cancer, thyroid cancer, and melanoma
Rumeng Zhang et al., Biomol Biomed, 2024

Supplemental data

Supplemental data are available at the following link: <https://www.bjbms.org/ojs/index.php/bjbms/article/view/12444/3874>.

Table S1. Relevant primer sequences for qRT-PCR

| Gene | Primer sequences | |
|------------|------------------|----------------------------------|
| WFDC3 | Forward | 5' - TCGGATCTGCCGAGACATTCT -3' |
| | Reverse | 5' - CTACACAGCTTTGTTGCAGCC -3' |
| GAPDH | Forward | 5' - GTCTCCTCTGACTTCAACAGCG -3' |
| | Reverse | 5' - ACCACCCTGTTGCTGTAGCCAA -3' |
| Perforin | Forward | 5' - GGGATTCCAGAGCCCAAGTG -3' |
| | Reverse | 5' - CAGCAGCAGGAGAAGGATGC -3' |
| Granzyme B | Forward | 5' - TGGGGGACCCAGAGATTAATA -3' |
| | Reverse | 5' - TTTCTCCATAGGAGACAATGC -3' |
| Granulysin | Forward | 5' - CAGGCTCCCTGCCATAATA -3' |
| | Reverse | 5' - CTCAAGCCTGGGTTGCC -3' |
| IFNG | Forward | 5' - GGGTTCTCTTGCTGTACTG -3' |
| | Reverse | 5' - TTTCTGTCACTCTCCTTTCC -3' |
| IL-2 | Forward | 5' - AGAACTCAAACCTCTGGAGGAAG -3' |
| | Reverse | 5' - GCTGTCTCATCAGCATATTACAC -3' |

WFDC: Whey acidic protein four-disulfide core; qRT-PCR: Quantitative real-time PCR.

Table S2. Antibodies for Western blot and IF

| Antibody | Manufacture | Item number | Species |
|----------------------------|--------------------------------|--------------------|----------------|
| WFDC3 | Immunoway, USA | Cat#YN7483 | Rabbit |
| ZO-1 | Cell Signaling Technology, USA | Cat#13663S | Rabbit |
| N-Cadherin | Cell Signaling Technology, USA | Cat#14215S | Mouse |
| E-Cadherin | Cell Signaling Technology, USA | Cat#14472S | Mouse |
| Vimentin | Cell Signaling Technology, USA | Cat#5741S | Rabbit |
| Snail | Cell Signaling Technology, USA | Cat#3879S | Rabbit |
| GAPDH | Cell Signaling Technology, USA | Cat#2118S | Rabbit |
| Goat anti-mouse IgG | ZSGB-BIO, China | Cat#ZB-2305 | Goat |
| Goat anti-rabbit IgG | ZSGB-BIO, China | Cat#ZB-2301 | Goat |
| FITC-goat anti-mouse IgG | ZSGB-BIO, China | Cat#ZF-0312 | Goat |
| TRITC-goat anti-rabbit IgG | ZSGB-BIO, China | Cat#ZF-0316 | Goat |

WFDC: Whey acidic protein four-disulfide core; IF: Immunofluorescence.